JOURNAL OF NEUROPHYSIOLOGY
Vol. 71, No. 2, February 1994. *Printed in U.S.A.*

Comparative Transduction Mechanisms of Hair Cells in the Bullfrog Utriculus. I. Responses to Intracellular Current

RICHARD A. BAIRD
Department of Neuro-otology and R. S. Dow Neurological Sciences Institute, Good Samaritan Hospital and Medical Center, Portland, Oregon 97209

SUMMARY AND CONCLUSIONS

1. Hair cells in whole-mount in vitro preparations of the utricular macula of the bullfrog (*Rana catesbeiana*) were selected according to their macular location and hair bundle morphology. The voltage responses of selected hair cells to intracellular current steps and sinusoids in the frequency range of 0.5–200 Hz were studied with conventional intracellular recordings.

2. The utricular macula is divided into medial and lateral parts by the striola, a 75- to 100-μm zone that runs for nearly the entire length of the sensory macula near its lateral border. The striola is distinguished from flanking extrastriolar regions by the elevated height of its apical surface and the wider spacing of its hair cells. A line dividing hair cells of opposing polarities, located near the lateral border of the striola, separates it into medial and lateral parts. On average, the striola consists of five to seven medial and two to three lateral rows of hair cells.

3. Utricular hair cells were classified into four types on the basis of hair bundle morphology. Type B cells, the predominant hair cell type in the utricular macula, are small cells with short stereocilia and kinocilia 2–6 times as long as their longest stereocilia. These hair cells were found throughout the extrastriola and, more rarely, in the striolar region. Three other hair cell types were restricted to the striolar region. Type C cells, found primarily in the outer striolar rows, resemble enlarged versions of Type B hair cells. Type F cells have kinocilia approximately equal in length to their longest stereocilia and are restricted to the middle striolar rows. Type E cells, found only in the innermost striolar rows, have short kinocilia with prominent kinociliary bulbs.

4. The resting potential of 99 hair cells was -58.0 ± 7.6 (SD) mV and did not vary significantly for hair cells in differing macular locations or with differing hair bundle morphology. The R_N of hair cells, measured from the voltage response to current steps, varied from 200 to >2,000 MΩ and was not well correlated with cell size. On average, Type B cells had the highest R_N, followed by Type F, Type E, and Type C cells. When normalized to their surface area, the membrane resistance of hair cells ranged from <1,000 to >10,000 k$\Omega \cdot cm^2$. The input capacitance of hair cells ranged from <3 to >15 pA, corresponding on average to a membrane capacitance of 0.8 ± 0.2 pA/cm^2.

5. The current-voltage (*I-V*) relations of utricular hair cells were correlated with their hair bundle morphology. Type B cells, in both the striolar ($n = 4$) and extrastriolar ($n = 3$) regions, had slightly outwardly rectifying *I-V* relations. The *I-V* relations of Type C cells ($n = 15$) were nearly linear for both depolarizing and hyperpolarizing currents. Type F cells ($n = 19$) had sigmoidal *I-V* relations that saturated for larger depolarizing and hyperpolarizing currents. Type E cells ($n = 14$), in addition to being outwardly rectifying at depolarizing currents, had a pronounced inward (anomalous) rectification for voltages more negative than -100 mV.

6. The voltage responses of Type B cells to intracellular current were largely passive. Hair cells restricted to the striolar region, on the other hand, exhibited active voltage responses at the onset and termination of depolarizing currents. The voltage responses of Type C cells were fast, peaking in 10–15 ms, and did not vary with current amplitude. Type F cells had slower responses, peaking in 25–50 ms. Most Type E cells, unlike other utricular hair cells, were electrically resonant, exhibiting one to three cycles of highly damped oscillations at the onset of depolarizing and the termination of hyperpolarizing current steps. A few Type E cells displayed spikelike responses.

7. To simulate the in vivo situation during hair bundle stimulation I examined the voltage responses of utricular hair cells to sinusoidal currents in the frequency range of 0.5–200 Hz. Type B and Type C cells had nearly linear responses for a wide range of stimulus amplitudes. Type E and, to a lesser extent, Type F cells displayed large nonlinear deviations during the depolarizing portion of their response. These deviations were most evident at low stimulus frequencies and their peak shifted with increasing frequency in individual cells.

8. My results suggest that utricular hair cells differ in their complements of basolateral membrane conductances. These conductances modify the sensitivity and response dynamics of hair cells to natural stimulation. Type B and Type F cells, for example, have high R_N and are dominated by slow potassium currents, suggesting that they encode tonic head movement. Type C cells, on the other hand, have low R_N and faster membrane currents, enabling them to encode phasic head movements over a wide range of amplitudes and frequencies. Type E cells are electrically resonating and presumably enable the bullfrog utriculus to encode substrate-borne vibration.

9. The utricular macula is organized to encode both tonic and dynamic displacement. Hair cells in extrastriolar regions possess only low-frequency sensitivity and presumably encode static gravity and tonic head movements. Hair cell types restricted to the striola, on the other hand, are adapted to encode high-frequency information. Within this dynamic zone there is a segregation of function, with Type C cells in the outer striolar rows providing dynamic gravity sensitivity and Type E cells in the innermost rows supplying vibratory sensitivity.

INTRODUCTION

Hair cells, the receptor cells of the vestibular otolith organs, encode information about the amplitude, frequency, and direction of static gravity and dynamic linear accelerations, including sound, substrate-borne vibration, and head and body movement (Hudspeth 1986). Receptor potentials from auditory (Crawford and Fettiplace 1981; Dallos 1986; Nutall 1985; Russell et al. 1986) and vestibular (Corey and Hudspeth 1979, 1983; Hudspeth and Corey 1977; Ohmori 1984) hair cells have provided important information concerning the first stages of sensory processing in these important cells. With few exceptions, however,

previous studies of mechanoelectric transduction in otolith hair cells have been confined to the bullfrog sacculus (for reviews, see Howard et al. 1988; Hudspeth 1986; Roberts et al. 1988). In the bullfrog this endorgan is a sensor of substrate-borne vibration (Koyama et al. 1982; Lewis et al. 1982). Little is known about comparative hair cell transduction mechanisms in other otolith endorgans, particularly those that possess static gravity sensitivity.

Hair cells in the bullfrog sacculus are specifically adapted to sense small-amplitude, high-frequency linear accelerations. Not surprisingly, these hair cells display many properties that are undesirable or inappropriate for hair cells that must provide static gravity sensitivity. The receptor currents of saccular hair cells, for example, adapt to maintained displacements of their hair bundles, sharply limiting their low-frequency sensitivity (Eatock et al. 1987). Saccular hair cells also exhibit an electrical resonance to intracellular current or hair bundle displacement (Ashmore 1983; Hudspeth and Lewis 1988a; Lewis and Hudspeth 1983). This phenomenon, determined by the interplay of basolateral calcium and calcium-activated potassium conductances (Hudspeth and Lewis 1988b), further sharpens the response of saccular hair cells to high frequencies.

I was interested in seeing how the transduction mechanisms of hair cells in a gravity-sensing otolith endorgan would differ from those in the bullfrog sacculus. The bullfrog utriculus is an appropriate model for these studies, because its structure is representative of higher vertebrates in general (Lindeman 1969; Wersall and Bagger-Sjoback 1974) and its function as a sensor of static gravity and dynamic linear acceleration is well known (Baird and Lewis 1986; Lewis et al. 1982). Hair cells in the bullfrog utriculus, classifiable as Type II by cell body and synapse morphology, differ markedly in hair bundle morphology from those in the bullfrog sacculus (Baird and Lewis 1986; Lewis and Li 1975). Moreover, the hair bundle morphologies of utricular hair cells, unlike those in the sacculus, differ in different membrane regions.

Recent studies in both the semicircular canals (Baird et al. 1988; Boyle et al. 1991; Goldberg et al. 1985; Honrubia et al. 1981, 1989) and the otolith endorgans (Goldberg et al. 1990) in a wide variety of vertebrate species have used morphophysiological techniques to relate the response properties of vestibular nerve afferents to their terminal morphology. These studies have shown that many of the discharge properties of vestibular afferents, including their sensitivity and response dynamics to natural stimulation, are correlated with their epithelial location. In particular, the vestibular endorgans are regionally organized, with afferents innervating the central zones of these endorgans having higher sensitivities and more phasic response dynamics than afferents supplying their peripheral zone. In mammals the sensitivities of vestibular afferents are determined by both their terminal morphology (Baird et al. 1988; Goldberg et al. 1985, 1990) and their postsynaptic recovery processes (Goldberg et al. 1984). Differences in response dynamics, on the other hand, appear to be solely determined by regional variations in presynaptic transduction mechanisms (Baird et al. 1988; Goldberg et al. 1985, 1990). In the semicircular canal, regional variations in cupular dynamics (Boyle et al. 1991; Hillman and McLaren 1979; Honrubia et al. 1981, 1989; McLaren and Hillman 1979) or the coupling of the cupula to the sensory hair bundles of hair cells (Honrubia et al. 1981, 1989; Lim 1976) may underlie the diversity in response dynamics. In the otolith organs, on the other hand, differences in afferent response dynamics may be determined by differences in the transduction properties of different hair cell types. In the bullfrog utriculus the response dynamics of utricular afferents are correlated with the hair bundle morphology of their innervated hair cells (Baird and Lewis 1986), suggesting that hair cells with differing hair bundle morphology may represent independent hair cell types with distinctive physiological response properties.

To test this hypothesis I selected utricular hair cells according to their macular location and hair bundle morphology and recorded their sensitivity and response dynamics to intracellular current and, in a companion study (Baird 1994), to hair bundle displacement. These recordings were made in whole-mount in vitro preparations of the bullfrog utriculus to preserve the macular location of utricular hair cells. Intracellular recordings were made with conventional microelectrodes because whole-cell patch-clamp recordings of hair cells are extremely difficult from the apical surface (Holton and Hudspeth 1986). The primary aim of this study was to see whether hair cells differing in their macular location or hair bundle morphology differed in their membrane properties or voltage responses to intracellular current. I was particularly interested in assessing, as in recent studies of auditory and vibratory hair cells (Art et al. 1986; Ashmore 1983; Crawford and Fettiplace 1981; Fuchs et al. 1988; Lewis and Hudspeth 1983; Pitchford and Ashmore 1987), whether electrical resonance contributed to frequency tuning in utricular hair cells and, if so, whether such resonance was restricted to hair cells located in particular macular regions (Art and Fettiplace 1987; Roberts et al. 1986) or possessing specific hair bundle morphologies (Fuchs et al. 1988; Sugihara and Furukawa 1989). I also hoped to determine how the transduction mechanisms of different hair cell types might contribute to differences in sensitivity and response dynamics among vestibular afferents.

My results reveal that the utriculus is highly organized, with utricular hair cells in different macular regions varying markedly in their voltage responses to intracellular current. In particular, hair cells in the central, or striolar, region of the utriculus have faster membrane currents than hair cells supplying the peripheral zone. Hair cells that differ in hair bundle morphology also differ in their passive and active membrane properties, suggesting that these cells differ in their complement of basolateral membrane conductances. One hair cell type, restricted to the innermost striola, displays electrical resonance. This resonance, unlike that seen in saccular hair cells (Ashmore 1983; Hudspeth and Lewis 1988a; Lewis and Hudspeth 1983), is highly damped and is similar in many ways to that observed in pigeon semicircular canal hair cells (Correia et al. 1989) and the toadfish sacculus (Steinacker and Romero 1992).

Preliminary accounts of portions of this data have been presented in abstract (Baird and Schuff 1990, 1991) and short manuscript form (Baird 1992).

METHODS

Isolation of the utricular macula

Adult bullfrogs (*Rana catesbiana*), weighing 100–150 g, were anesthetized with 0.2% MS-222 (Sigma) and decapitated. The decapitated head was placed in cold, oxygenated artificial saline containing (in mM) 110 Na^+, 2 K^+, 4 Ca^{2+}, 120 Cl^-, 3 D-Glucose and 5 *N*-2-hydroxyethylpiperazine-*N'*-2-ethanesulfonic acid, pH 7.25. The osmotic strength of this solution, measured with a freezing-point osmometer (Fiske), was 220–240 mOsm. While in the above solution the membranous labyrinth was exposed and the utricular maculae were dissected free of the vestibular nerves and the horizontal and anterior vertical semicircular canals. Utricular maculae were stored in cold, oxygenated artificial saline for ≤8 h. Immediately before intracellular recordings the otolith membrane was removed by gentle mechanical agitation after enzymatically digesting the utricular macula for 30–45 min in 50 μg/ml subtilopeptidase BPN' (Sigma). Excised maculae were trimmed of excess nerve to improve the visibility of hair bundles and bisected perpendicularly to the striola with a Teflon-coated double-edged razor blade. Macular pieces were then mounted flat, hair cells uppermost, in a small chamber on the fixed stage of an upright microscope (Zeiss, model 16) and perfused at a rate of 0.2–0.5 ml/min with oxygenated saline maintained at room temperature (20–22°C). The preparation was protected from radiant heating with an infrared filter in the microscope illumination system.

Identification of utricular hair cells

Before attempting intracellular recordings I visualized the apical surface of the utricular macula with a ×40 water-immersion objective (Zeiss). The striolar region was identified from its characteristic ribbon-shaped appearance (Fig. 1, *A* and *B*) and divided, by the polarization of its constituent hair cells, into medial and lateral parts. Using Nomarski optics and a contrast-enhancement video camera (Hamamatsu, C2400), utricular hair cells were viewed from above and recorded on videotape with an S-VHS videocassette recorder (Panasonic, PV-S4864).

Hair cells were identified by macular location and hair bundle morphology. Hair cells were first assigned to the medial or lateral side of the striolar or extrastriolar region. The position of hair cells within the extrastriolar regions was measured from the medial or lateral striolar border. Striolar hair cells, depending on their relative distance from the line dividing hair cells of opposing polarities, were placed into one of three categories. Hair cells immediately adjacent to this line were assigned to the inner striolar rows. Hair cells adjacent to the medial and lateral extrastriolar region were described as being in the outer striolar rows. The remaining striolar hair cells were assigned to the middle striolar rows. I did not measure the position of hair cells parallel to the long axis of the striola. Selected hair cells were generally located in the broad central region of the macula (Fig. 1*A*).

With my optics I could just resolve the component kinocilia and stereocilia of striolar hair cells (Fig. 1*B*). Hair bundle morphology was characterized by the size of the hair bundle, the presence or absence of a bulbed kinocilium, and the relative lengths of the kinocilium and longest stereocilia. The latter two discriminations were made by gently separating the kinocilium from the stereociliary array with a fine glass probe. In pilot experiments, my on-line identification of hair cell morphology was verified by labeling selected hair cells with Lucifer yellow (Stewart 1978) or biocytin (Horikawa and Armstrong 1988) microelectrodes and corroborating their hair bundle morphology in sectioned material. Dye-filled microelectrodes were not routinely used because of the capriciousness of dye ejection from high-resistance microelectrodes.

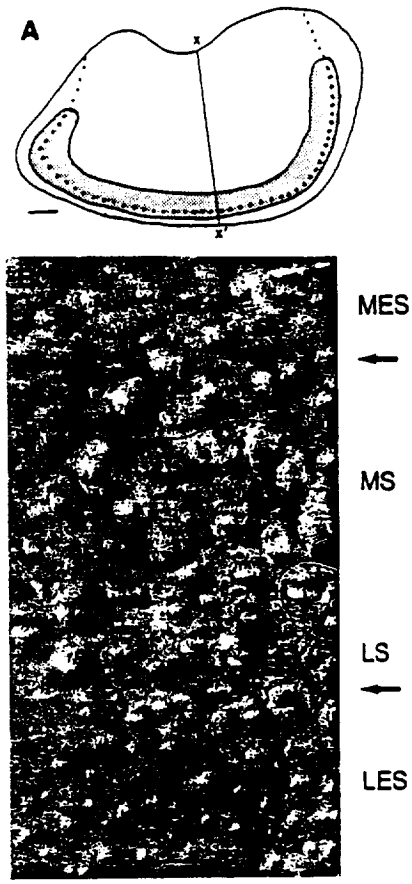

FIG. 1. *A*: surface reconstruction of the whole-mount utricular macula. Crosses with solid line: plane of section seen in Fig. 2. The striola (shaded area), a narrow ribbon-shaped zone, and its anterior and posterior extensions (dotted lines) separate the extrastriola into medial and lateral parts. Bar: 100 μm. *B*: Nomarski photomicrograph of the utricular striola and surrounding extrastriolar regions. Arrows: medial (*top*) and lateral (*bottom*) borders of the striolar region. Dotted line: reversal of hair cell polarization. MES, medial extrastriola; MS, medial striola; LS, lateral striola; LES, lateral extrastriola. Bar: 25 μm.

Intracellular recordings

Intracellular recordings were performed with glass microelectrodes pulled from thin-walled aluminosilicate glass (A-M Systems) and bent at 45–90° angles 200–250 μm from their tips to allow nearly vertical penetrations of the apical surfaces of hair cells (Hudspeth and Corey 1977). The shanks of microelectrodes were coated with silicone plastic (Dow Corning, Sylgard 184) to increase mechanical strength and reduce capacitance. In some experiments microelectrode tips were dipped briefly in 100 μg/ml streptomycin sulfate (Sigma) immediately before use to improve the quality of intracellular recordings (Holton and Hudspeth 1986). Recording microelectrodes were filled with 3 M KCl and had resistances between 150 and 300 MΩ. Microelectrodes with time constants >250 μs were discarded. The remaining microelectrodes were checked for their ability to pass depolarizing and hyperpolarizing currents in the range of ±1 nA in a linear manner. Responses to larger currents were corrected for microelectrode characteristics.

Intracellular voltage responses were recorded with an Axoclamp-2A amplifier (Axon Instruments) operating in continuous bridge mode. Voltage outputs from the Axoclamp-2A amplifier, stimulus waveforms, and internal sync marks were recorded and stored on videotape (Instrutech). These waveforms were also digi-

tally sampled at 10 kHz, stored on hard disk, and analyzed on- and off-line with a DEC LSI 11/73 microcomputer.

The responses of hair cells to intracellular current were first determined from their steady-state and dynamic voltage responses to 100-ms depolarizing and hyperpolarizing current steps. Microelectrodes were balanced in the saline bath before impaling and immediately after withdrawing from hair cells. On some occasions it was necessary to readjust the bridge balance intracellularly to cancel a fast component in the voltage responses. This fast component, which had a fast (<1 ms) time constant and a symmetrical response to depolarizing and hyperpolarizing current steps, was attributed to the electrode resistance. The slower components of voltage responses were attributed to the hair cell membrane.

The responses of hair cells to intracellular current were averages of results obtained in response to 16 stimulus presentations. Current steps were usually alternated between hyperpolarizing and depolarizing values, starting at −10 to −40 pA and increasing current amplitude by 10 or 20 pA at each iteration. In a few experiments hair cells were depolarized or hyperpolarized with constant current before the presentation of current steps. Steady-state voltage responses were measured 50–100 ms from the onset of current steps and used to calculate the steady-state current-voltage (*I-V*) relations of utricular hair cells. R_N was measured with small (−10 to −40 pA) hyperpolarizing current steps and determined from the slope of the best-fitting regression line through the linear portion of the *I-V* relation. Steady-state slope conductances were determined over a 40-mV range depolarizing and hyperpolarizing to resting membrane potential. The membrane time constant (t_m) was estimated from the slowest component of the voltage response to a hyperpolarizing current step. Voltage responses were rejected for this purpose if *1*) they did not fall in the linear portion of the *I-V* relation, *2*) they displayed a significant sag after their initial hyperpolarizing response, or *3*) time constants for the response at the onset and offset of the current step were significantly different. Input capacitance (C_N) was calculated from the relation $C_N = t_m/R_N$.

Sinusoidal stimuli were superimposed with small (10–40 pA) depolarizing bias currents and delivered to the recording microelectrode by a function generator (Wavetek, model 185). I then examined the voltage responses of hair cells to sinusoidal current using individual sinusoids and logarithmic frequency sweeps. In the latter case hair cells were stimulated at a start frequency (0.5 or 5.0 Hz) for several cycles. Sinusoidal current was then logarithmically swept over a low (0.5–20) or high (5.0–200 Hz) frequency range, during which frequency was increased between the start and end frequencies in 10 equally spaced discrete steps. For individual sinusoids the number of rotation cycles was matched to the frequency of oscillation to maintain an equal duration of stimulation for each experimental condition. Responses to successive sine wave cycles were averaged; the number of cycles was matched to stimulus frequency, varying from 2 at 0.5 Hz to 16 at 200 Hz. Cycle histograms were created by plotting for discrete frequencies the averaged voltage responses versus the stimulus cycle. The peak-to-peak amplitude of sinusoidal currents was varied from 10 to 100 pA, producing a maximum voltage response of ~5–20 mV.

Morphological analyses

Four utricular maculae were fixed for 2 h in 4.0% paraformaldehyde in 0.1 M phosphate buffer, rinsed in 0.1 M phosphate buffer, dehydrated in a series of ethanol solutions, and mounted in depression slides. Under low magnification the boundaries of the sensory macula and the striolar region were input to a computerized image analysis system (Bioquant, system IV). At higher magnification hair cell density in representative macular areas was determined by counting the number of hair cells within a 100 × 75 μm rectangle. Within each endorgan four measurements were made across the anterior-to-posterior extent of the macula and averaged to obtain a mean value for hair cell density in the striolar and medial and lateral extrastriolar zones. I then averaged these measures across animals for each macular zone. In the striolar region the outlines of individual hair cells were traced. Whole-mount maculae were then rinsed briefly in xylene and absolute ethanol, embedded in glycol methacrylate (Polysciences, JB-4), and serially sectioned at 8 μm in a coronal plane.

Sectioned material was examined with ×40 and ×63 oil immersion objectives under bright-field illumination. Individual hair cells in the striolar and extrastriolar regions were classified according to their hair bundle morphology. For each hair cell measurements were made of hair bundle diameter and the lengths of the kinocilium and shortest and longest stereocilia. Estimates of the total surface area of hair cells were made by modeling hair cells as idealized spheres and/or cylinders (Fig. 2, *middle*). The diameter of spherical cells was measured and the surface area calculated as $A = 4\pi r^2$. For cylindrical hair cells the longitudinal axis was measured and measurements of the horizontal axis at 2 to 5-μm intervals from the apical surface were averaged to calculate hair cell diameter. The surface area of cylindrical hair cells was then calculated as $A = 2\pi r(r + h)$. In a few cases the apical and basal portions of hair cells were modeled using a combined cylinder-sphere model. The surface area of these cells was approximated by the formula $A = 2\pi(r_1 h + 2r_2^2)$, where r_1 and r_2 were the radii of the cylindrical and spherical portions of the cell, respectively. For each hair cell type the average contribution of the stereociliary membrane to total surface area was calculated using a cylindrical model and mean values of stereocilia number, diameter, and length obtained from a separate population of hair cells (see Table 1, Baird 1994).

Statistical procedures

Unless otherwise stated statistical comparisons of morphometric data were based on a one-way analysis of variance. Where appropriate, post hoc pairwise multiple comparisons were performed using the Tukey multiple comparison test adjusting, when necessary, for unequal group sizes (Miller 1977).

RESULTS

Organization of the utricular macula

The utricular macula of the bullfrog, as in other vertebrates, is a kidney-shaped structure (Fernandez et al. 1990; Lindeman 1969; Wersall and Bagger-Sjoback 1974). The posterior part of the sensory epithelium lies in a horizontal plane. Its anterior part, as in mammals, is curved upward. The utricular macula in the bullfrog is divided into a large medial and a smaller lateral region by the striola, a narrow zone of distinctive morphology that runs for most of the length of the sensory epithelium near its lateral border (Fig. 1*A*).

The striola, a 75- to 100-μm-wide ribbon-shaped zone, differed in several respects from flanking extrastriolar regions. Some of these differences can be appreciated from the photomicrographs of Figs. 1 and 2. Hair cells in the striola tended to be larger and more widely spaced than hair cells in the medial or lateral extrastriola (Fig. 1*B*). The density of hair cells in the striolar region of four animals was 0.018 ± 0.002 (SD) hair cells per μm^2. Hair cell density in the medial and lateral extrastriola was significantly

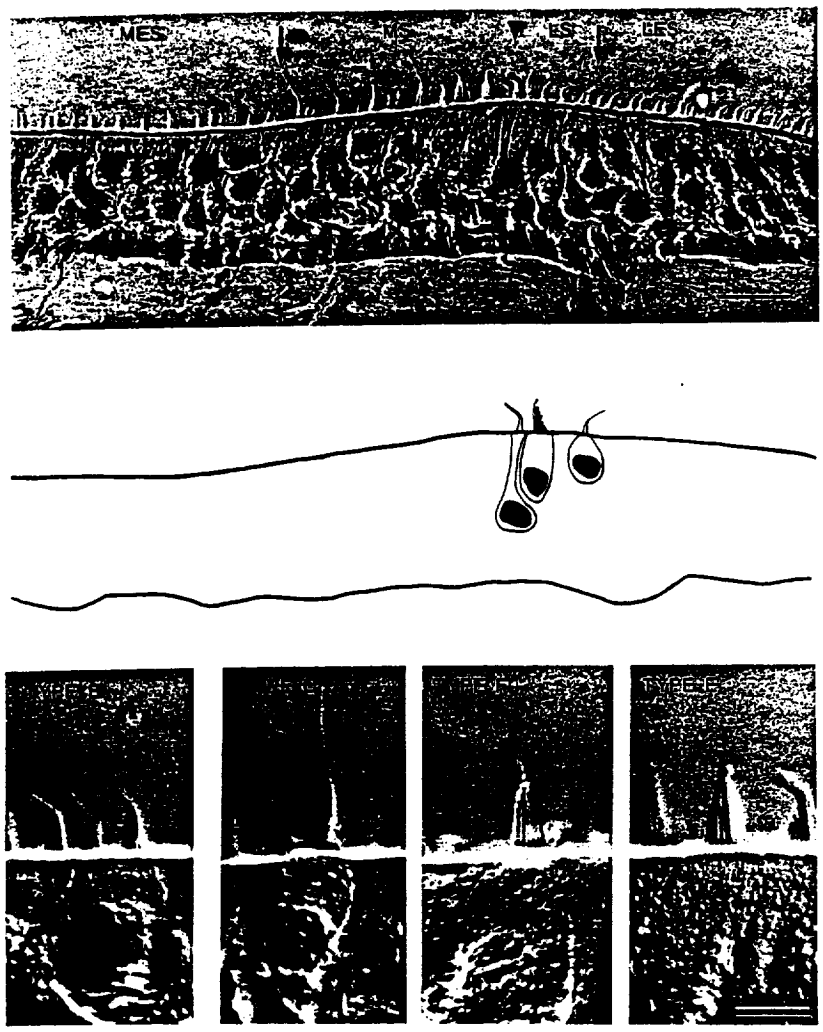

FIG. 2. Nomarski photomicrograph (*top*) and schematic sketch (*middle*) of toluidine-blue stained cross-section of the utricular macula, indicating the cellular morphology of representative hair cells in the utricular macula. Outer arrows: medial (*left*) and lateral (*right*) borders of the striolar region. Pointer: reversal of hair cell polarization. *Bottom*: Nomarski photomicrographs of the hair bundles of individual hair cells in the extrastriolar (*left*) and striolar (*right*) regions. Bars: 25 μm (*top* and *middle*); 10 μm (*bottom*).

higher, averaging 0.030 ± 0.002 and 0.047 ± 0.005, respectively. In sectioned material the apical surface of the striola was higher in elevation than that of the surrounding extrastriolar regions, giving the striola a hill-like appearance (Fig. 2, *top*). Finally, most hair cells in the striolar region (Fig. 2, *bottom right*) were larger and had different hair bundle morphologies than hair cells located in the extrastriolar regions (Fig. 2, *bottom left*).

The boundaries between the striolar region and the medial and lateral extrasriola were easily recognized in whole-mount (Fig. 1*B*) and sectioned (Fig. 2, *top*) material. In either extrastriolar region the orientation of hair cells was directed toward the striolar region. Hair cells in the striolar region were oriented in the same direction as adjacent extrastriolar cells. A line dividing hair cells of opposing polarities, located near the lateral border of the striola, further separated the striola into medial and lateral rows (dotted line, Fig. 1, *A* and *B*; pointer, Fig. 2, *top*). On average, the striola consisted of five to seven medial rows and two to three lateral rows of hair cells (Figs. 1*B* and 2, *top*). For the remainder of this paper I will refer to the portion of the striola bordering the line dividing hair cells of opposing polarities as the inner rows, that adjacent to the medial or lateral extrastriola as the outer rows, and the remainder of the striola as the middle rows.

Morphological characteristics of utricular hair cells

Utricular hair cells, following the original scheme of Lewis and Li (1975), were classified into four types by hair bundle morphology (Fig. 2, *bottom*). Type B cells, the predominant hair cell type in the utricular macula, had small apical surfaces and short stereocilia, with kinocilia 2–6 times as long as their longest stereocilia (Fig. 2, *bottom left*). Three other hair cell types had a variety of surface morphologies, with stereocilia markedly longer than those of Type B cells (Fig. 2, *bottom right*). Type C cells resembled an enlarged version of Type B cells, having kinocilia and stereocilia approximately twice as large as the latter hair cell type. The remaining two hair cell types had kinocilia equal or slightly longer in length than their longest stereocilia, significantly shorter than the kinocilia of Type B and Type C cells. Type F cells had visibly larger hair bundles than other utricular hair cells. Type E cells had smaller hair bundles and, unlike Type F cells, prominent kinociliary bulbs.

With the exception of Type F cells the great majority of utricular hair cells had cylindrical cell bodies. This was particularly true of Type E cells, which uniformly had cylindrical cell bodies. The majority (14/23 = 60.9%) of Type F cells, by contrast, had spherical cell bodies. The cell bodies of Type B and Type C cells were a function of their macular

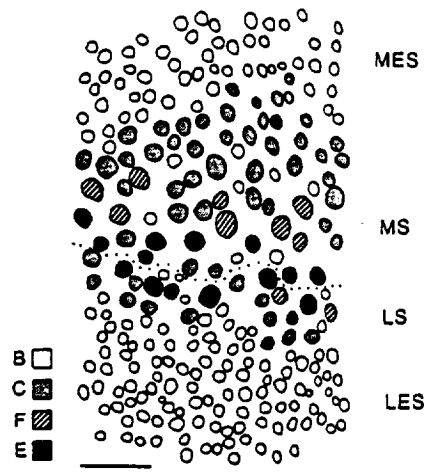

FIG. 3. Macular distribution of hair cell types in the utricular macula. Dotted line: reversal of hair cell polarization. Bar: 25 μm.

location. Type B cells in extrastriolar regions, including 22 of 30 in the medial extrastriola and 16 of 19 in the lateral extrastriola, had cylindrical cell bodies. The cell bodies of 5 of 6 striolar Type B cells, on the other hand, were best described by a cylinder-sphere model. Type C cells had cylindrical (22/41 = 53.7%) or spherical (11/41 = 26.8%) cell bodies, depending on whether they were located in the outer or inner striolar rows.

The macular distribution of the above hair cell types in a typical utricular macula is depicted in Fig. 3. Type B cells were found throughout the medial and lateral extrastriola and, more rarely, in the striolar region. The remaining three hair cell types were confined to the striolar region. Type C cells were found throughout the striola but were particularly numerous in the outer striolar rows. Moving inward, these hair cells were gradually replaced by Type F cells. The latter hair cells, unlike Type C cells, were restricted to the middle striolar rows. Type E cells were seen only in the innermost striolar rows, lying astride both sides of the line dividing hair cells of opposing polarities. In four animals extrastriolar Type B cells were estimated to make up 87.8 ± 3.4% of utricular hair cells. Of 365 striolar hair cells identified in my morphological studies, 54 (20.4%) were Type B, 132 (49.8%) were Type C, 24 (9.0%) were Type F, and 55 (20.8%) were Type E.

The morphological characteristics of 135 utricular hair cells and regional variations among the hair cell types are summarized in Table 1. The legend to Table 1 also summarizes the results of statistical tests. Hair cells in the utriculus differed markedly in their lengths and apical diameters. As a group Type B hair cells had the smallest apical diameters of utricular hair cells. Type B cells in the striolar and lateral extrastriolar regions had significantly smaller apical diameters and longer lengths than Type B cells in the medial extrastriolar region. There was, however, no significant difference in surface area between Type B cells in different macular regions ($P > 0.5$). With the exception of Type B cells, hair cells in the striolar region were larger in diameter and surface area than hair cells in the medial extrastriola. Among both Type C and Type F cells, hair cells in the inner striolar rows tended to be smaller in diameter and longer in length than their counterparts in the outer striolar rows. Type B and Type E hair cells, both of which were largely restricted to the inner rows, were also significantly longer in length than other utricular hair cells.

Hair cell types in the utriculus also differed dramatically in the lengths of their constituent kinocilia and stereocilia. The shortest and longest stereocilia of Type B and Type C cells were shorter than those of Type F and Type E cells. The kinocilia and the longest, but not the shortest, stereocilia of Type C cells were also significantly longer than those of Type B cells. Among Type B cells, hair cells in the striola had somewhat shorter kinocilia and stereocilia than those in the medial and lateral extrastriola. With the exception of Type B cells, regional differences among hair cell types were small and statistically insignificant.

Passive membrane properties of utricular hair cells

The responses of 99 utricular hair cells were examined with intracellular current steps. Of this total 8 (8.1%) were Type B cells located in the medial ($n = 7$) or lateral ($n = 1$) extrastriola within 100 μm of the striolar region. The remaining 91 (91.9%) hair cells were located within the striolar region. Of these 6 (6.6%) were Type B, 28 (30.8%) were Type C, 35 (38.4%) were Type F, and 22 (24.2%) were Type E. Not surprisingly, my intracellular recordings were biased toward sampling from hair cells with larger apical surfaces. Thus Type F cells, the largest utricular hair cells, were overrepresented and Type B cells, the smallest utricular hair cells, were underrepresented in my physiological sample. This was particularly true for Type B cells from the striola and lateral extrastriola.

The passive membrane properties of utricular hair cells are summarized in Table 2. The resting membrane potentials of all 99 hair cells ranged from −40 to −75 mV (−58.0 ± 7.6 mV, mean ± SD). There was no significant difference in the resting membrane potential of hair cells located in different macular zones. The resting membrane potentials of hair cells in the striolar region, for example, were similar to those of hair cells in the medial and lateral extrastriolar regions ($P > 0.2$). There was also no significant difference in the resting membrane potentials of different hair cell types ($P > 0.2$). By contrast, the R_N and t_m of hair cells varied markedly for different hair cell types. Type C cells had the lowest R_N (236 ± 40 MΩ) and time constants (2.7 ± 1.1 ms) of all utricular hair cells. Type B cells, whether in the striola or extrastriola, had R_N (1764 ± 768 MΩ) and time constants (8.2 ± 3.0 ms) consistently higher than those of other hair cells. The C_N of utricular hair cells was calculated from the relation $C_N = t_m/R_N$ and varied from <2 to >20 pF.

The specific membrane resistance and capacitance of utricular hair cells were estimated by normalizing the R_N and capacitance of individual cells to the mean surface areas of hair cell types (Table 2). Because hair cell types also differed in the number and size of their stereocilia, the contribution of the stereociliary array to membrane surface area was included in this calculation (Table 1, Baird 1994). When normalized to their surface area the r_m of utricular hair cells ranged from <1,500 to >15,000 kΩ · cm^2 and was lowest for Type C cells and highest for Type F cells. Mean

TABLE 1. *Morphological properties of utricular hair cells*

Cell Type	n	Hair Cell: Diameter, μm	Hair Cell: Length, μm	Hair Cell: Surface Area, μm²	Stereociliary Length: Shortest, μm	Stereociliary Length: Longest, μm	Kinociliary Length, μm
Type B	55	4.5 ± 1.1	13.6 ± 4.1	383.1 ± 70.3	1.1 ± 0.5	3.8 ± 1.0	12.2 ± 1.9
MES	30	5.2 ± 0.9	11.5 ± 3.0	385.3 ± 64.8	1.2 ± 0.5	4.0 ± 0.9	12.6 ± 1.6
MS/LS	6	3.4 ± 0.3	20.0 ± 5.1	373.5 ± 68.0	0.7 ± 0.4	2.8 ± 0.4	10.3 ± 1.9
LES	19	3.9 ± 0.8	15.0 ± 2.4	382.6 ± 82.1	1.1 ± 0.4	3.9 ± 1.0	12.1 ± 2.0
Type C	41	5.1 ± 0.8	12.4 ± 3.8	556.9 ± 113.5	1.3 ± 0.6	6.3 ± 1.2	16.6 ± 2.3
Type F	23	7.0 ± 1.4	13.1 ± 3.7	1106.3 ± 181.9	1.9 ± 0.9	8.2 ± 1.3	9.3 ± 1.2
Type E	16	6.3 ± 1.6	21.9 ± 3.5	805.0 ± 111.2	2.1 ± 0.7	8.9 ± 1.1	9.8 ± 1.1

Values are means ± SD; *n* is number of hair cells. Surface area calculated using a cylinder ($SA = 2\pi r(r + h)$), sphere ($SA = 4\pi r^2$), or cylinder and sphere ($SA = 2\pi(r_1 h + 2r_2^2)$) model, as appropriate, and includes the mean contribution of the stereociliary membrane. The following differences were statistically significant. Hair cell diameter: Type F vs. Types C and B, Type E vs. Type B, MES Type B vs. LES Type B, $P < 0.001$; MES Type B vs. striolar Type B, $P < 0.005$; Type E vs. Type C, $P < 0.05$. Hair cell length: Type E vs. Types F, B, and C, Striolar Type B vs. MES Type B, $P < 0.001$; LES Type B vs. MES Type B, $P < 0.01$; striolar Type B vs. LES Type B, $P < 0.05$. Surface area: Types F and E vs. Types C and B, MES Type B vs. LES Type B, $P < 0.001$ in all cases; Type F vs. Type E, Type C vs. Type B, $P < 0.005$. Shortest stereociliary length: Type E vs. Types C and B, Type F vs. Type B, $P < 0.001$; Type F vs. Type C, $P < 0.005$. Longest stereociliary length: Types E and F vs. Types C and B, Type C vs. Type B, $P < 0.001$ in all cases. Kinociliary length: Types C and B vs. Types E and F, Type C vs. Type B, $P < 0.001$ in all cases. MES, medial extrastriola; MS, medial striola; LS, lateral striola; LES, lateral extrastriola.

membrane capacitance varied from 0.6 μF/cm² for Type F cells to 2.1 μF/cm² for Type C cells.

Voltage responses to intracellular current steps

RESPONSES TO DEPOLARIZING CURRENTS. The voltage responses of all utricular hair cells were similar for small depolarizing currents. There were marked differences, however, in the voltage responses of hair cells to larger depolarizing currents. These differences were not strongly correlated with macular location. Hair cells with similar hair bundle morphology, on the other hand, had similar voltage responses regardless of their macular location. This is clearly seen in Fig. 4, which illustrates the voltage responses of typical Type B, Type C, and Type F cells to intracellular current steps. In Type B cells depolarizing currents largely produced passive exponential changes in membrane potential, although some evidence of active potential changes were seen for large depolarizing currents (Fig. 4, *top left*). Active potential changes were more commonly seen in Type C (Fig. 4, *top right*) and Type F (Fig. 4, *bottom left*) cells, resulting in depolarizing peaks with associated decreases in slope resistance. These peaks were evoked from resting membrane potential by depolarizing current steps and their size was graded with current amplitude. Active potential changes in Type C cells were uniformly small (Fig. 4, *top right*). These changes had rapid onsets, with time-to-peak values <10 ms, and slightly slower decay times. The size of these peaks did not decrease at large positive potentials. Type F cells typically exhibited larger and slower (>25 ms) potential changes, which decayed more slowly to steady-state values (Fig. 4, *bottom left*). Unlike Type C cells, the peaks of Type F decreased in size for voltages more positive than −10 mv. Type F cells also displayed a small hyperpolarizing undershoot at the termination of depolarizing current steps. Five Type F cells, with more outwardly rectifying *I-V* relations (open circles and open squares, Fig. 6), had more rapid onsets and decays than typical Type F cells. Three of these cells (Fig. 4, *bottom middle*), all located in the outer striolar rows, had voltage responses to depolarizing current resembling those of Type C cells. These cells had smaller, more rapid onsets

TABLE 2. *Passive membrane properties of utricular hair cells*

Cell Type	n	Membrane Potential, mV	n	Resistance: Input, MΩ	Resistance: Membrane, kΩ/cm²	Time Constant, ms	Capacitance: Input, pF	Capacitance: Membrane, μF/cm²
Type B	14	−59.3 ± 7.7	8	1764 ± 768	6690 ± 2924	8.17 ± 3.00	4.86 ± 2.20	1.29 ± 0.59
MES	7	−60.1 ± 7.7	3	1960 ± 648	7552 ± 2497	6.66 ± 3.38	3.72 ± 1.14	0.96 ± 0.30
MS/LS	6	−58.8 ± 8.8	5	1606 ± 890	6000 ± 3330	9.30 ± 2.43	5.71 ± 2.55	1.53 ± 0.68
LES	1	−55.9	0	—	—	—	—	—
Type C	28	−58.7 ± 8.1	18	236 ± 40	1313 ± 225	2.70 ± 1.08	11.61 ± 4.69	2.08 ± 0.84
Type F	35	−57.8 ± 7.2	22	908 ± 417	10043 ± 4609	5.44 ± 1.79	6.91 ± 3.18	0.62 ± 0.29
Type E	22	−56.7 ± 7.7	18	366 ± 143	4011 ± 1626	5.18 ± 2.76	14.73 ± 6.63	1.83 ± 0.82

Values are means ± SD; *n* is number of hair cells. Input resistance (R_N) is average resistance over the range of −100 to −60 mV. Membrane time constant is determined from the voltage response to a hyperpolarizing current step (−10 to −40 pA, 100 ms duration). Input capacitance (C_N) is calculated by dividing the membrane time constant by the input resistance. Specific membrane resistance, (r_m) and specific membrane capacitance (c_m) calculated from $r_m = R_N \cdot SA$ and $c_m = C_N/SA$, where SA is mean surface area. The following differences were statistically significant. Input resistance: Type B vs. Types F, E, and C, Type F vs. Types E and C, $P < 0.001$. Membrane resistance: Type F vs. Types E and C, Type B vs. Type C, $P < 0.001$; Type F vs. Type B, Type E vs. Type C, $P < 0.05$. Input capacitance: Type E vs. Types F and B, $P < 0.001$; Type C vs. Types F and B, $P < 0.05$. Membrane capacitance: Types C and E vs. Type F, $P < 0.001$; Type C vs. Type B, $P < 0.05$. For abbreviations, see Table 1.

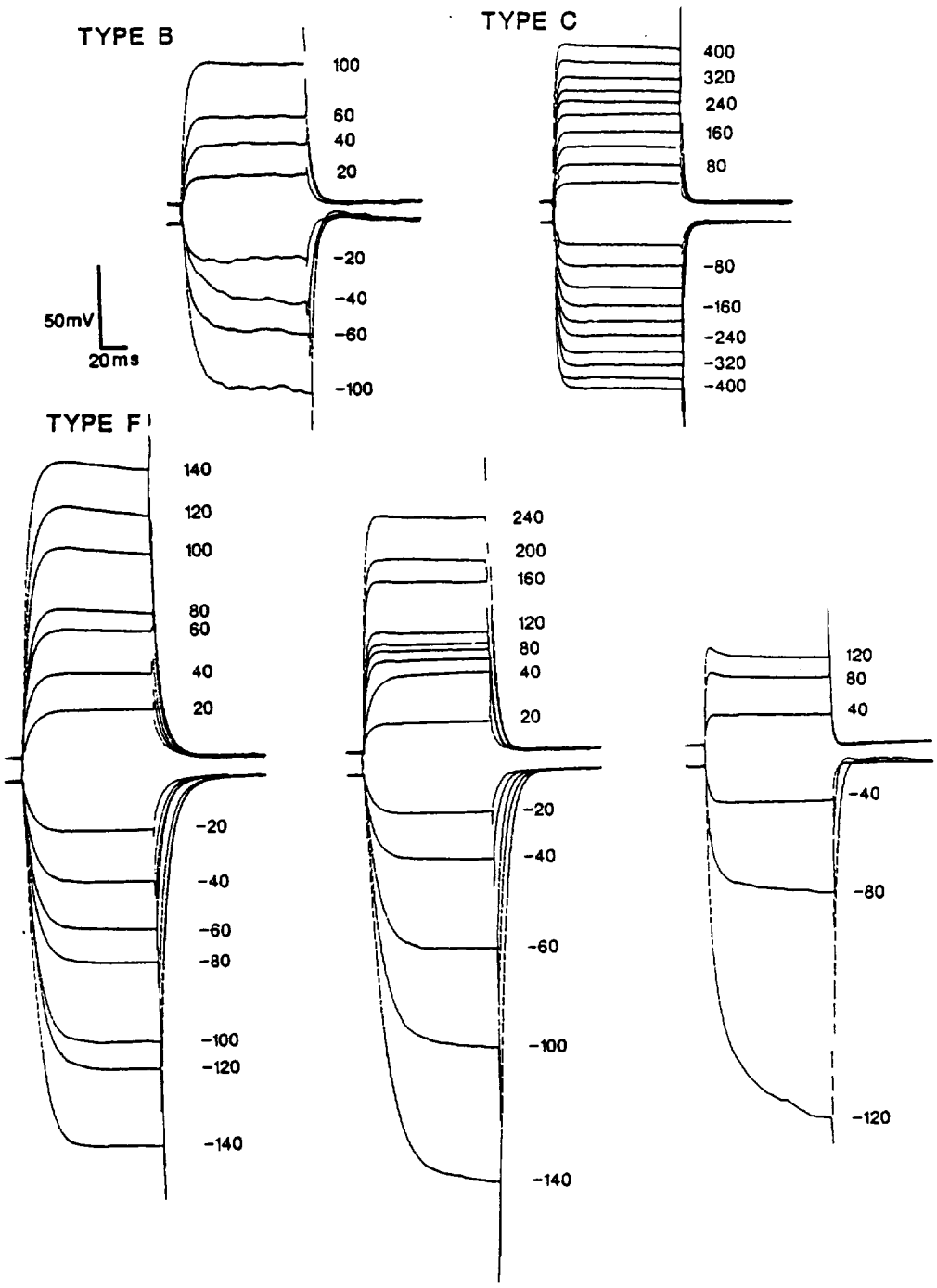

FIG. 4. Voltage responses of Type B (*top left*), Type C (*top right*), and Type F (*bottom left*) hair cells to 100-ms depolarizing and hyperpolarizing current steps of varying amplitude. Also shown are the voltage responses of 2 transitional Type F hair cells (*bottom middle* and *bottom right*). Numbers to the *right* of each trace are the amplitude of the step stimulus (picoamperes).

and a smaller hyperpolarizing undershoot at the termination of depolarizing steps than most Type F cells. Two other Type F cells (Fig. 4, *bottom right*) had voltage responses resembling those of Type E cells, with large, rapid onsets and a large hyperpolarizing undershoot at the termination of depolarizing steps. These cells were both located in the inner striolar rows.

Termination of the depolarizing peaks of Type C and Type F cells could result from the inactivation of a transient membrane conductance, the delayed activation of an inactivating membrane conductance, or both. The linearity of the I-V relation for long times and the lack of a substantial hyperpolarizing undershoot at the end of depolarizing current steps suggests that the termination of the depolarizing peak was the result of a transient conductance change. This suggestion is supported by the results of experiments in which hair cells were held at depolarized or hyperpolarized membrane potentials by the injection of constant

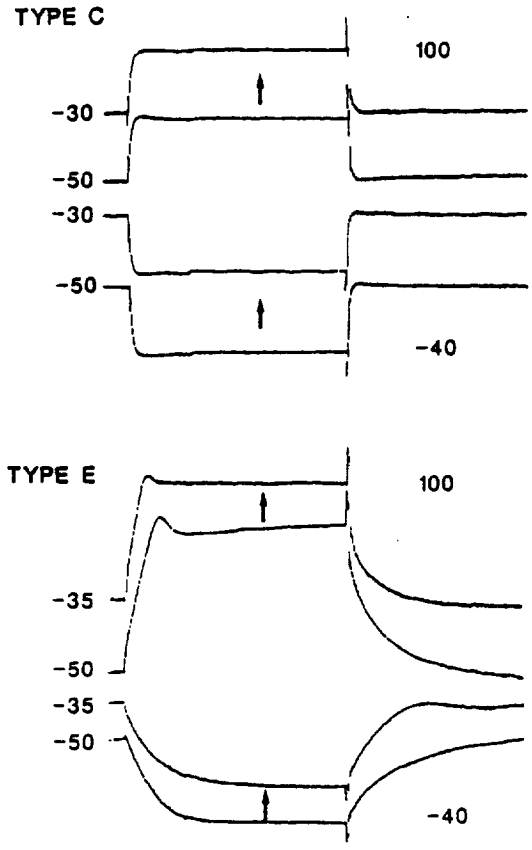

FIG. 5. Voltage responses of a Type C (*top*) and Type E (*bottom*) hair cell held at depolarizing membrane potentials to depolarizing and hyperpolarizing current steps. Numbers to the *left* of each trace indicate resting membrane potential (millivolts); numbers to the *right* are the amplitude of the step stimulus (picoamperes).

current (Fig. 5). In these experiments the depolarizing peaks of Type C cells were reduced in response to depolarizing current steps (Fig. 5, *top*). Similarly, these peaks were increased when cells were held at hyperpolarizing membrane potentials (data not shown), suggesting that the time course of the depolarizing peak largely results from inactivation of membrane current at depolarized membrane potentials.

RESPONSES TO HYPERPOLARIZING CURRENTS. The responses of Type B cells to hyperpolarizing currents differed in two ways from those to depolarizing currents. One, hyperpolarizing currents produced slightly larger responses than depolarizing currents. Two, a rebound depolarization was observed at the termination of the current step. In response to similar currents, Type C cells displayed both a small sag in membrane potential from an initial maximum and a rebound depolarization at the termination of the current step. This rebound depolarization and, to a lesser extent, the sag were smaller in Type C cells with more depolarized resting membrane potentials and were decreased in amplitude by direct current depolarization (Fig. 5, *top*). Type F cells, unlike Type C cells, did not display sags or rebound depolarizations at the end of a hyperpolarizing current step. Rather, hyperpolarizing current steps caused large, slow potential changes in these hair cells, suggesting a strongly rectifying *I-V* relationship.

Steady-state I-V relations

The steady-state *I-V* relations of all utricular hair cells were relatively linear near resting potential. There were marked differences, however, in the voltage responses of hair cells at large depolarizing and hyperpolarizing currents. This is clearly seen in Fig. 6, which shows the steady-state *I-V* relations of 55 hair cells that were recorded at four or more values of intracellular current. Type B cells, in both the striola ($n = 4$) and medial extrastriola ($n = 3$), had slightly outwardly rectifying *I-V* relations, with slope conductances varying from 0.59 ± 0.39 nS for hyperpolarizing currents to 0.81 ± 0.42 nS for depolarizing currents (Fig. 6, *top*). I was unable to obtain the *I-V* relations of Type B cells in the lateral extrastriola. Type C cells ($n = 15$) had nearly linear *I-V* relations and higher slope conductances (Fig. 6, *top middle*). As expected, the conductances of these cells to depolarizing currents were only slightly different from those to hyperpolarizing currents (5.06 ± 1.10 and 4.49 ± 0.86 nS, respectively). Type F cells ($n = 19$), on the other hand, had strongly outwardly rectifying *I-V* relations, with slope conductances of 1.33 ± 0.52 nS for hyperpolarizing currents and 1.94 ± 0.84 nS for depolarizing currents (Fig. 6, *bottom middle*). Most Type F cells had sigmoidal *I-V* relations that saturated for large depolarizing currents (open triangles). Other Type F cells, located in the outer (open squares) or inner (open circles) striolar rows, displayed outward rectification near resting membrane potential and did not saturate for larger positive currents. Type E cells ($n = 14$) were also strongly outwardly rectifying for depolarizing currents, with slope conductances of 3.29 ± 1.06 nS for hyperpolarizing currents and 4.27 ± 1.24 nS for depolarizing currents. In addition, they displayed a pronounced inward (or anomalous) rectification for membrane potentials more negative than approximately −100 mV (Fig. 6, *bottom*).

Electrical resonance

Most (19/22) Type E cells, unlike other utricular hair cells, were electrically resonant, producing one to three cycles of heavily damped oscillations (ringing) at the onset of depolarizing current steps. The membrane potentials of these hair cells rapidly decreased to a steady-state plateau that was maintained throughout the current step (Fig. 7, *left*). The amplitude, frequency, and quality of ringing at the onset of the current step initially increased with depolarizing current. Larger depolarizing currents increased only the first voltage peak, resulting in a disappearance of subsequent peaks and converting the ringing into a spike-like response. At the termination of depolarizing current steps, resonating Type E cells rapidly repolarized to resting levels with no hyperpolarizing undershoot.

A few (3/22) Type E cells did not exhibit ringing for any value of intracellular current. Rather, they had only spike-like responses, displaying prominent depolarizing peaks in response to depolarizing current steps. In these cells the membrane potential became increasingly depolarized toward the end of the current step (Fig. 7, *right*). The amplitude of both the depolarizing peak and the increasing membrane depolarization seen in these cells was reduced when they were held at depolarized membrane potentials by the

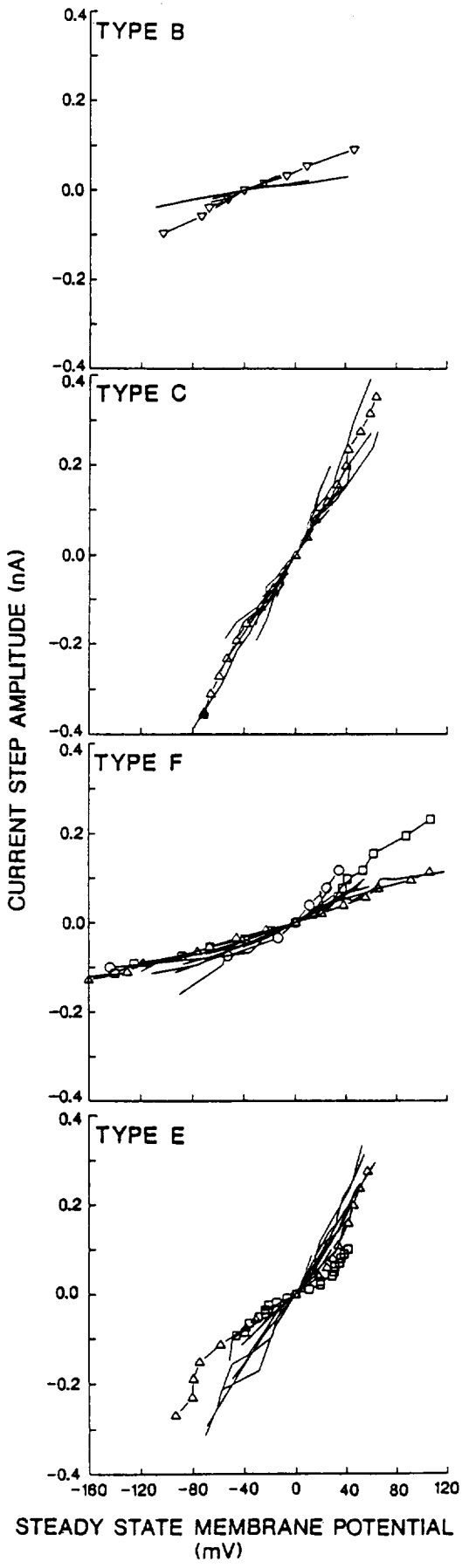

injection of constant current (Fig. 5, *bottom*). The repolarization of spiking Type E cells at the termination of depolarizing current steps was significantly slower than that of resonating Type E cells (Fig. 7, *right*).

Hyperpolarizing currents produced, as in Type C cells, a sag in membrane potential from an initial maximum with no associated oscillations (Fig. 7, *left* and *right*). This sag was reduced in amplitude by direct current depolarization (Fig. 5, *bottom*). In resonating Type E cells (Fig. 7, *left*) oscillations were also seen after the termination of the current step. These oscillations were of lower frequency than those seen at the onset of depolarizing currents. Similar oscillations were also seen in spiking Type E cells depolarized with direct current (Fig. 5, *bottom*).

I was interested in comparing the responses of electrically resonant hair cells in the utriculus with those in the bullfrog sacculus, a preparation in which the ionic basis of such resonance is better understood. The responses of saccular hair cells, like those of utricular hair cells, fell into two classes. In most (10/12) saccular hair cells decaying oscillations were observed in response to depolarizing current steps. These oscillations were superimposed on a steady-state plateau and were symmetrical, i.e., ringing occurred at both the onset and termination of the current step (Fig. 8*A*). The frequency of oscillations after depolarizing currents was largely independent of current amplitude and was a measure of the cell's natural frequency (Crawford and Fettiplace 1981; Lewis and Hudspeth 1983). As in utricular hair cells the amplitude, frequency, and quality of ringing at the onset of the current step initially increased with depolarizing current. Larger depolarizing currents increased only the first voltage peak, resulting in a disappearance of subsequent peaks and converting the ringing into a spikelike response. Two hair cells, both located at the peripheral margins of the sacculus, displayed spikelike responses to depolarizing current (Fig. 8*B*). The membrane potential of these cells slowly repolarized after removal of the depolarizing current, exhibiting a prominent slow hyperpolarizing undershoot at the termination of the current step. Hyperpolarizing current steps caused large potential changes in all saccular hair cells with no associated oscillations, suggesting a strongly rectifying *I-V* relationship (Fig. 8, *A* and *B*). Oscillatory changes were, however, observed at the termination of hyperpolarizing current steps. As in utricular hair cells these oscillations were of a lower frequency than those seen at the onset of depolarizing currents.

As expected, the steady-state *I-V* relations of utricular and saccular hair cells were similar. This can be seen in Fig. 9, which illustrates the steady-state *I-V* relations of 14 utricular (Fig. 9*A*) and 12 saccular (Fig. 9*B*) hair cells recorded at four or more values of intracellular current. As in the sacculus most utricular hair cells displayed some degree of

FIG. 6. Steady-state current-voltage (*I-V*) relations, measured 100 ms after the onset of an intracellularly injected current step, for 7 Type B, 15 Type C, 19 Type F, and 14 Type E hair cells. Symbols indicate the steady-state *I-V* relations of hair cells whose voltage responses are shown in Figs. 5 (Types B, C, and F) and 7 (Type E). Triangles: Type B, Type C, Type F, and resonant Type E hair cells. Circles: transitional Type F hair cells. Squares: transitional Type F or spiking Type E hair cells.

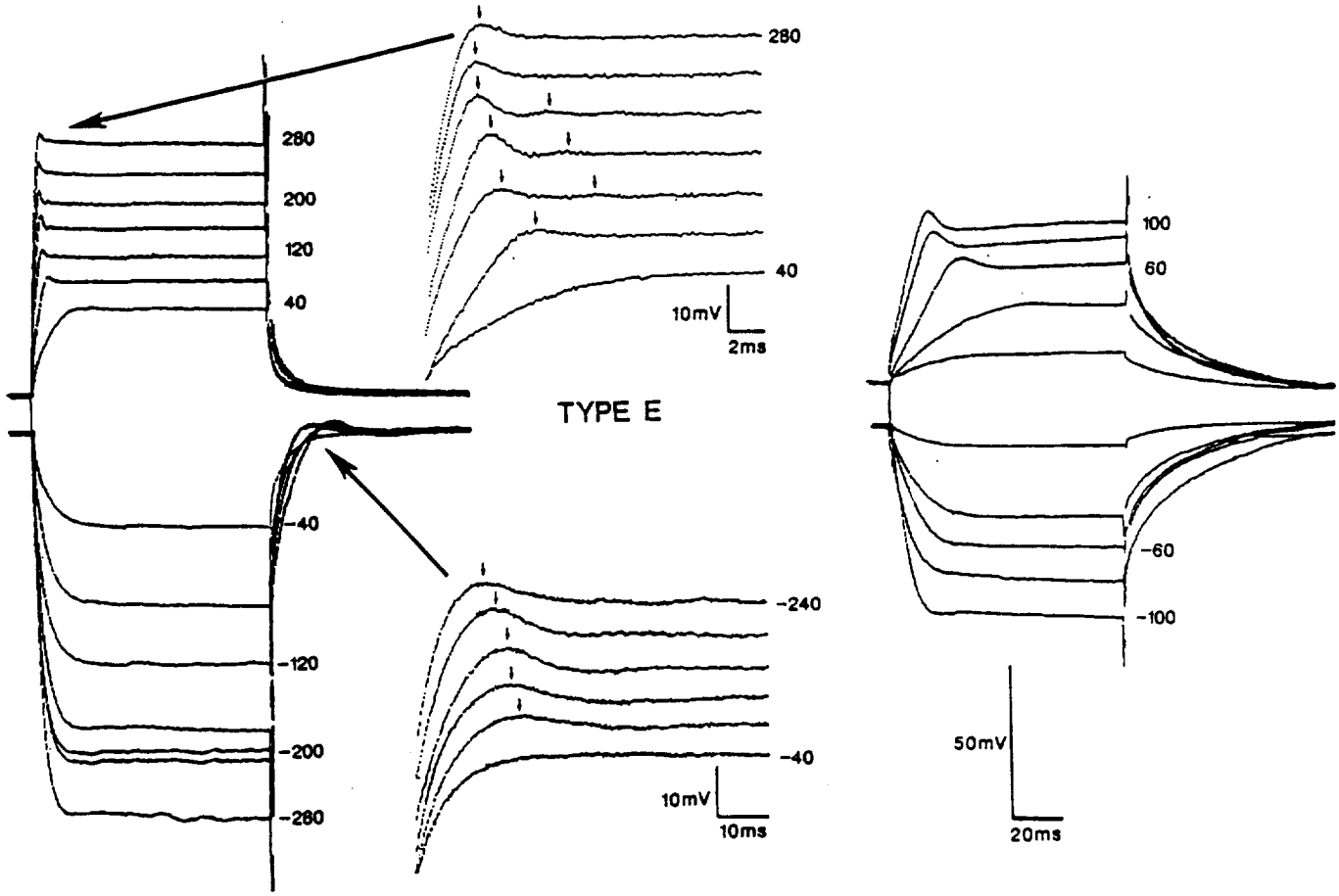

FIG. 7. Voltage responses of resonant (*left*) and spiking (*right*) Type E hair cells to depolarizing and hyperpolarizing current steps of varying amplitude. Numbers to the *right* of selected traces are the amplitude of the step stimulus (picoamperes). Detailed *insets* of membrane oscillations at the onset of depolarizing and the termination of hyperpolarizing current are shown to the *right* of the resonant Type E cell. Small arrows in the detailed *insets*: occurrence of peaks in the oscillatory voltage response.

inward (or anomalous) rectification for membrane potentials more negative than approximately −100 mV. In addition, both utricular and saccular hair cells were strongly outwardly rectifying for depolarizing voltages. The slope conductances of utricular hair cells to hyperpolarizing currents were only slightly different from those of saccular hair cells (3.29 ± 1.06 and 4.22 ± 1.22 nS, respectively). The slope conductances of utricular cells to depolarizing currents, on the other hand, were significantly lower than those of saccular cells, measuring 4.27 ± 1.24 and 8.75 ± 3.55 nS, respectively. Spiking hair cells (squares) in both endorgans had lower slope conductances to depolarizing currents than resonating cells (triangles).

Responses to intracellular current sinusoids

To simulate the in vivo stimulation of hair cells during hair bundle stimulation I examined the responses of utricular hair cells to sinusoidal current sweeps in the frequency range of 0.5–200 Hz. The passive membrane properties of hair cells determined from sinusoidal currents were similar to those determined from current steps. In particular, Type B and Type C cells, by virtue of their membrane time constants, had the smallest and largest bandwidths of all utricular hair cells. The responses of Type B cells were linear for a wide range of amplitudes (Fig. 10, *top*). This was also true to a lesser extent for Type C and Type F cells (data not shown). Type E cells, although linear at low stimulus amplitudes, were strongly rectifying at higher amplitudes, resulting in pronounced DC shifts at high frequencies (Fig. 10, *bottom*).

The voltage responses of utricular hair cells to individual current sinusoids were also examined. As expected, the responses of Type B (Fig. 11, *top*) and Type C (data not shown) cells displayed little or no distortion at any frequency. Type E and, to a lesser extent, Type F cells (data not shown) displayed large nonlinear deviations during the depolarizing portion of their sinusoidal response (Fig. 11, *middle*). These deviations, indicated by arrows in Fig. 11, were most evident at low stimulus frequencies, reaching a maximum at the resonant frequency of the cell and becoming successively smaller at higher frequencies. Within a given cell the peak of these deviations also shifted with increasing frequency, occuring at different portions of the stimulus cycle. This phenomenon was also observed in saccular hair cells, although nonlinear deviations in these cells were restricted to a smaller portion of the stimulus cycle than those of utricular hair cells at all stimulus frequencies (Fig. 11, *bottom*).

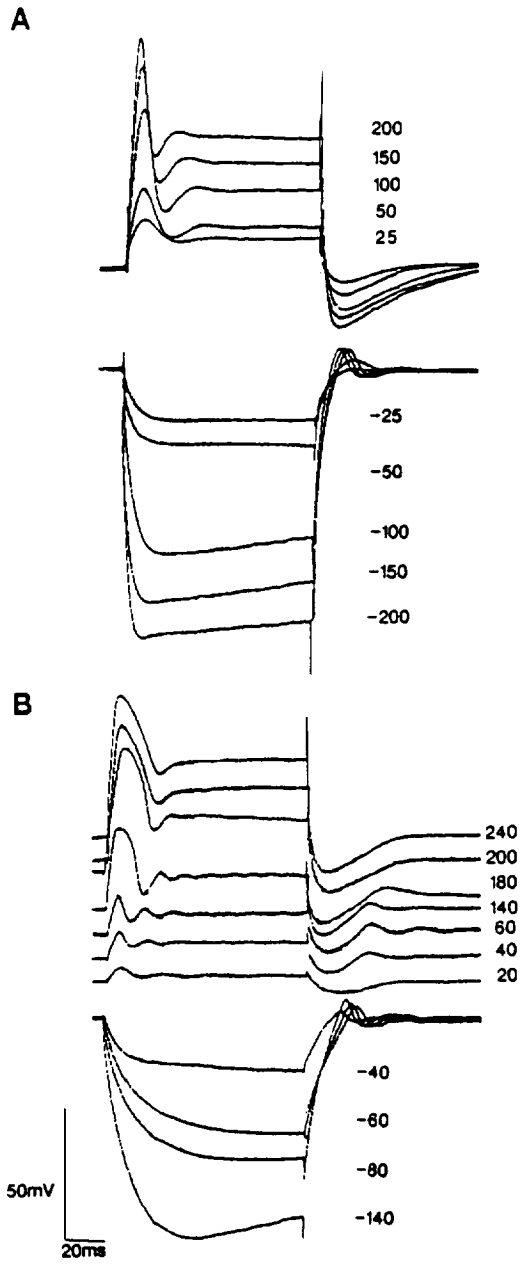

FIG. 8. Voltage responses of resonant (*A*) and spiking (*B*) saccular hair cells to depolarizing (*top*) and hyperpolarizing (*bottom*) current steps of varying amplitude. Numbers to the *right* of each trace are the amplitude of the step stimulus (picoamperes).

DISCUSSION

The results of the present study clearly demonstrate that hair cells in the bullfrog utriculus, identified as Type II by cell body and synapse morphology (Wersall and Bagger-Sjoback 1974), can be further classified into a number of types on the basis of hair bundle morphology. These hair cell types possess unique macular distributions. Recent studies have also shown that immature versions of these hair cell types exist in the regenerating bullfrog utriculus (Baird et al. 1994), suggesting that these cells may represent distinct phenotypes within the vestibular otolith organs. These hair cell types differ in their passive membrane properties and voltage responses to intracellular current, suggesting that they differ in their complement of basolateral membrane conductances. These conductances, by acting as frequency-dependent filters of the receptor current, determine how faithfully the membrane potential of hair cells follows their receptor current and modify the responses of hair cells to natural stimulation, regulating sensitivity, frequency selectivity, and synaptic release.

My results represent, to my knowledge, the first direct evidence of physiological differences being associated with differences in kinociliary and stereociliary morphology. There is already strong evidence that hair cells with differing cellular morphology differ in their physiological response properties. In the auditory system, for example, inner and outer hair cells in the mammalian cochlea express different ionic currents and respond differently to intracellular current (Brownell et al. 1985; Kros and Crawford 1990). A similar distinction is seen in the chick cochlea (Fuchs and Evans 1990; Murrow and Fuchs 1990), where hair cells have been divided according to cell body length into short and tall classes. In the vestibular system similar studies have shown that Type I and Type II hair cells in the pigeon (Lang and Correia 1989), guinea pig (Rennie and Ashmore 1991), and the rat (Eatock and Hutzler 1992) differ in their complement of basolateral membrane conductances. Sugihara and Furukawa (1989) have also shown that Type II hair cells in the goldfish sacculus can vary in

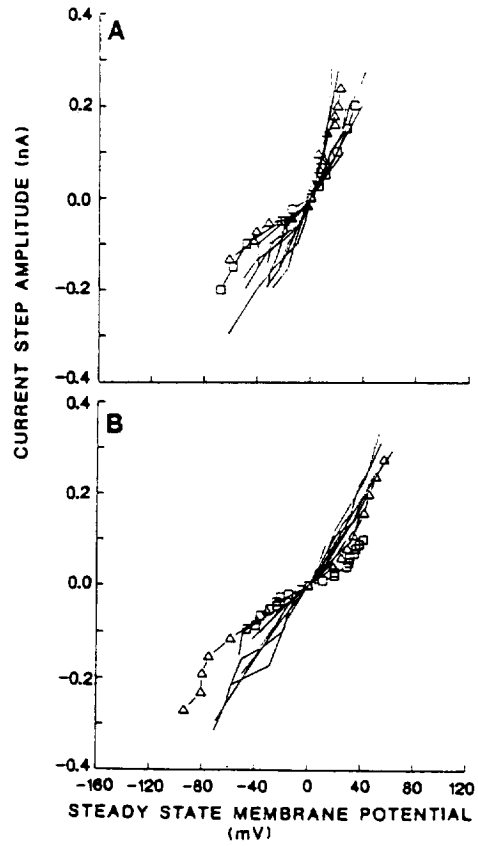

FIG. 9. Steady-state *I-V* relations measured 100 ms after the onset of an intracellularly injected current step, for 14 utricular Type E (*A*) and 12 saccular (*B*) hair cells. Symbols indicate the steady-state *I-V* relations of hair cells whose voltage responses are shown in Figs. 7 (utricular Type E) and 8 (saccular), respectively. Triangles: resonant hair cells. Squares: spiking hair cells.

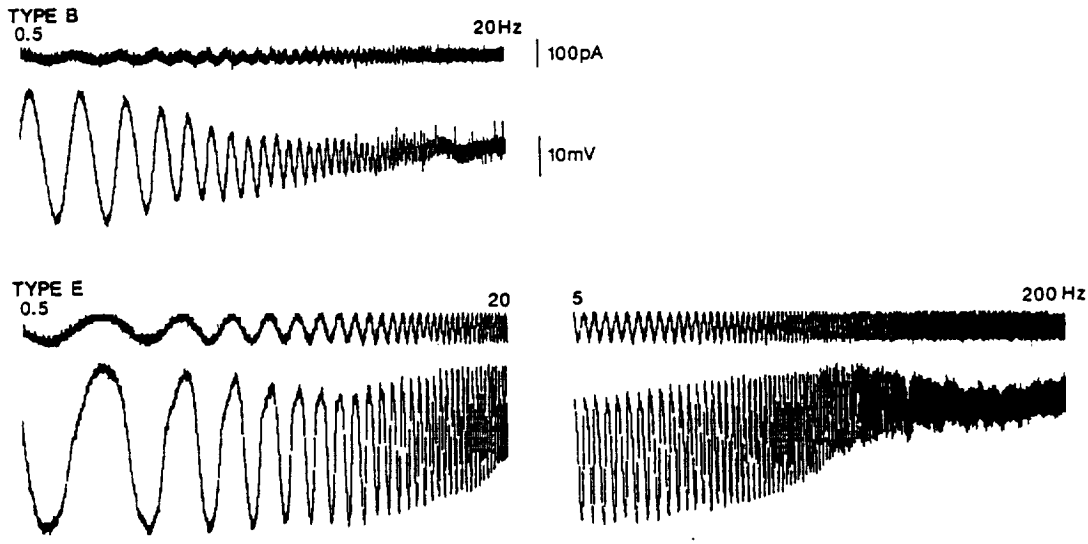

FIG. 10. Voltage responses of a Type B (*top*) and a resonant Type E (*bottom*) hair cell to logarithmic sweeps of sinusoidal current from 0.5 to 20 Hz (*left*) and 5 to 200 Hz (*right*). For each pair of waveforms *top trace*: current stimulus; *bottom trace*: resulting voltage response.

their physiological response properties, with short cells displaying oscillatory responses and tall cells displaying spike-like responses to intracellular current.

Previous studies have also demonstrated that hair cells with differing hair bundle morphology differ in their physiological response properties. The best frequencies of electrically tuned hair cells in the lizard (Turner et al. 1981) and turtle (Art and Fettiplace 1987) cochlea, for example, are correlated with their stereociliary lengths. Short and tall hair cells in the chick cochlea (Fuchs and Evans 1990; Murrow and Fuchs 1990) and the goldfish sacculus (Sugihara and Furukawa 1989) also differ, although not so systematically, in sterociliary length. In each case faster outward currents are associated with higher resonant frequencies and are found in hair cells with successively shorter stereociliary lengths.

Because hair cells in different epithelial regions often display subtle morphological differences it has proven difficult to unambiguously relate regional variations in physiological properties to different hair cell types. In the bullfrog utriculus, on the other hand, differences in hair bundle morphology are more marked than in other preparations and are only weakly correlated with differences in cellular morphology. Hair cells in the inner striola, for example, were significantly longer in length than those in the extrastriolar or outer striolar rows, regardless of their hair bundle morphology. Moreover, Type B cells, the only hair cell type found in all macular regions, had similar response properties in both the striolar and extrastriolar regions. Unfortunately only a small number of Type B cells were recorded in this study and these cells were all located within the striola or immediately adjacent to its medial border. A larger and more widely dispersed sample of these hair cells would be desirable. Finally, striolar hair cells in similar macular locations, but with different hair bundle morphology, differ in their physiological response properties. Interestingly, hair cells intermediate in their hair bundle morphology were also intermediate in their physiology. Some hair cells, for example, were difficult to classify because they had kinocilia longer than Type F but shorter than Type C cells. These hair cells had voltage responses resembling those of Type C cells for depolarizing currents and those of Type F cells for hyperpolarizing currents.

The cellular mechanism(s) by which hair cells link the development of the hair bundle and the expression of ionic currents in their basolateral membranes are not well understood. It is not difficult, however, to see why such a linkage would be desirable. First, the hair bundle contributes significantly to input capacitance and therefore to the membrane time constant of hair cells. Second, hair bundle morphology contributes to the sensitivity and, possibly, the frequency selectivity of the hair cell to natural stimulation. This point is explored more quantitatively in a companion paper (Baird 1994).

Passive membrane properties of utricular hair cells

Differences in the responses of utricular hair cells to intracellular current could reflect differences in the leakage conductance, passive membrane properties, or the basolateral membrane conductances of hair cell types. Resting membrane potential, for example, can influence the filtering properties of cells by determining the setpoint for the activation and inactivation of ionic channels. The mean resting membrane potential of utricular hair cells is similar to that reported for vestibular hair cells in the chick (Ohmori 1984) and Type II semicircular canal hair cells from the bullfrog (Housley et al. 1989), pigeon (Correia et al. 1989), guinea pig (Rennie and Ashmore 1991), and rat (Eatock and Hutzler 1992). Surprisingly, I did not observe a difference in the resting membrane potentials of different utricular hair cell types. In other preparations the resting membrane potentials of different hair cell types vary markedly. Short and long Type II hair cells in the goldfish sacculus, for example, have resting potentials of −78 and −101 mV, respectively (Sugihara and Furukawa 1989). In the pigeon semicircular canals Type I and Type II hair cells have resting membrane potentials of −70 and −57 mV,

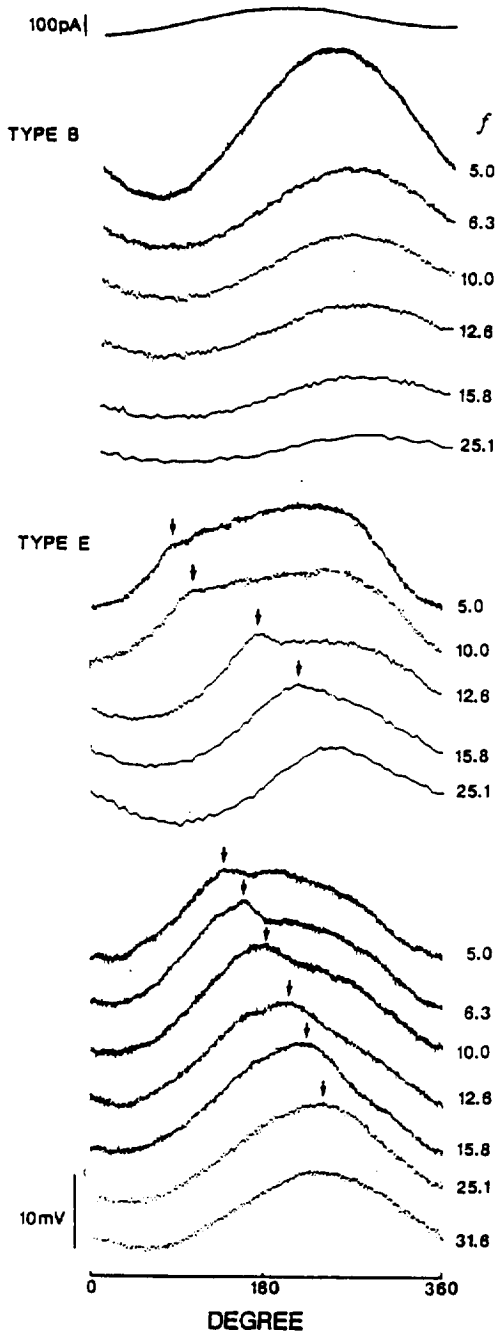

FIG. 11. Cycle histograms of the voltage responses of utricular Type B (*top*), utricular Type E (*middle*), and saccular (*bottom*) hair cells to sinusoidal current. Numbers to the *right* of each trace indicate the frequency of the sinusoidal current stimulus. Small arrows: peak distortion of the voltage response of utricular Type E (*middle*) and saccular (*bottom*) hair cells at each frequency.

respectively (Correia et al. 1989). Type I and Type II hair cells in the guinea pig (Rennie and Ashmore 1991) and rat (Eatock and Hutzler 1992), on the other hand, do not vary in resting membrane potential.

The sensitivity and frequency selectivity of hair cells are also partially determined by their passive membrane properties. R_N, along with input capacitance, determines the membrane time constant and the low-pass corner frequency of hair cells at low voltage levels. By determining the slope conductance around resting membrane potential R_N also determines the sensitivity of hair cells to receptor current. Type B cells, for example, have high R_N that limit their low-pass corner frequencies and give them low slope conductances to small receptor voltages. Type C cells, on the other hand, have low R_N, greatly increasing their slope conductance around resting membrane potential. R_N and slope conductance can also change dramatically as hair cells depolarize. In Type E and Type F cells, for example, slope conductance decreases markedly with increasing depolarization, increasing the corner frequencies of these hair cell types for larger stimulation.

My measurements of membrane resistance in utricular hair cells are almost certainly underestimates because they ignore the leakage resistance created by the intracellular impalement of cells by sharp microelectrodes. Using whole-cell patch-clamp recordings, mean R_N of 0.4 GΩ have been reported for Type I hair cells in the pigeon semicircular canals (Correia and Lang 1990). Values of R_N for Type II hair cells in the chick vestibular organs (Ohmori 1984) and the pigeon (Correia et al. 1989) and bullfrog (Housley et al. 1989) semicircular canal have been reported to range from 1 to 10 GΩ. With the use of conventional recording techniques, however, somewhat lower values of R_N have been reported by other investigators. In the bullfrog sacculus, for example, Hudspeth and Corey (1977) measured R_N of 200–900 MΩ, values in substantial agreement with my values for utricular hair cells. The input capacitances of utricular hair cells are also similar to those reported for other preparations, which for vestibular hair cells have ranged from 3 pF for hair cells in the bullfrog (Corey and Hudspeth 1983) and goldfish sacculus (Sugihara and Furukawa 1989) to 13 pF for Type II hair cells in the pigeon semicircular canal (Correia et al. 1989). As in other neural tissue, the specific membrane capacitance of hair cells appears to be ~1 $\mu F/cm^2$ (Housley et al. 1989; Ohmori 1984).

Type C hair cells had significantly lower R_N than other hair cell types. I considered the possibility that these cells were selectively damaged during isolation of the utricular macula. In early experiments it was observed that Type C cells were often selectively damaged by removal of the otolith membrane. This problem was avoided in later experiments by increasing the duration of enzymatic digestion. Although I did not attempt intracellular recordings from obviously damaged hair cells it is possible that some Type C cells were damaged by my isolation procedure. The resting membrane potentials of Type C cells, however, were not significantly different from those of other utricular hair cells. Furthermore, Type C cells, despite their low R_N, displayed normal responses to hair bundle stimulation (Baird 1994).

I also considered the possibility that differences in the R_N of hair cells were an artifact created by the impalement of these cells with sharp microelectrodes. Two lines of evidence suggest, however, that differences in R_N among hair cell types were not an artifact of my recording conditions. R_N, if governed by the shunt conductance created by microelectrode impalement, should be correlated with resting membrane potential. This was not observed. In addition, damage from microelectrode impalement might be expected to be greater in smaller than in larger hair cells. On

the contrary, Type B cells, which are significantly smaller than Type C cells, were found to have the highest R_N of all utricular hair cells.

Electrical resonance

Many utricular Type E cells were electrically resonant, displaying evoked oscillations of their membrane potential in response to depolarizing current steps. Electrical resonance was first demonstrated in the turtle cochlea (Crawford and Fettiplace 1981) and has since been demonstrated in the amphibian sacculus (Ashmore 1983; Hudspeth and Lewis 1988a; Lewis and Hudspeth 1983), amphibian papilla (Pitchford and Ashmore 1987), and chick cochlea (Fuchs et al. 1988). In these auditory and vibratory endorgans high-quality oscillations are evoked by intracellular current and natural stimulation. Electrical resonance seen in the goldfish and toadfish sacculus is of a somewhat lower quality (Steinacker and Romero 1992; Sugihara and Furukawa 1989). In the vestibular organs Housley et al. (1989) have reported electrical resonance in isolated bullfrog semicircular canal hair cells but only in response to extremely large (1.0 nA) intracellular currents. A study of electrical resonance in hair cells isolated from the pigeon semicircular canal, on the other hand, revealed that 59% of Type II hair cells had resonance peaks in their impedance functions or some form of membrane ringing for potentials near their resting membrane potential (Correia et al. 1989). More recently, Rennie and Ashmore (1991) and Eatock and Hutzler (1992) have reported that Type II, but not Type I, hair cells in the guinea pig and rat semicircular canal possess highly damped resonances to intracellular current.

The responses of Type E cells closely resemble the responses of oscillatory hair cells in the pigeon semicircular canal (Fig. 6, Lang and Correia 1989) and goldfish (Fig. 3, Sugihara and Furukawa 1989) and toadfish (Steinacker and Romero 1992) sacculus. As in these other preparations, two types of responses to depolarizing current are observed. The majority of Type E cells have fast responses and relatively high resonant frequencies. These cells, like oscillatory cells from the rostral goldfish sacculus (Sugihara and Furkawa 1989), display resonant responses at all depolarizing potentials, exhibiting rapid returns to resting membrane potential after a depolarizing current step. Other Type E cells respond to depolarizing current with slow, spikelike responses followed by a slowly increasing depolarization.

The quality of electrical oscillations in utricular hair cells is less than that seen in higher vertebrates. This is at least partially due to my use of sharp microelectrodes that, during impalement, introduce large leakage conductances into hair cells. Electrical oscillations in saccular hair cells, for example, are smaller and more highly damped in my recordings than in whole-cell patch-clamp recordings (Lewis and Hudspeth 1983; Hudspeth and Lewis 1988a). There are, nevertheless, several major differences in the responses of electrically resonant utricular and saccular hair cells under the same recording conditions. One, oscillatory potential changes in utricular hair cells are only produced by larger depolarizing currents than those needed to evoke similar changes in saccular hair cells. Two, these oscillations are smaller and more highly damped than those seen in saccular hair cells (cf. Figs. 7 and 8). Three, oscillations in utricular hair cells are always asymmetric, i.e., ringing is not seen in utricular hair cells at the termination of depolarizing current steps. Finally, unlike saccular hair cells, utricular hair cells do not exhibit hyperpolarizing undershoots at the termination of depolarizing current steps.

Presumptive membrane conductances of utricular hair cells

Several investigators have used the whole-cell variation of the patch-clamp technique (Hamill et al. 1981; Marty and Neher 1983) to study the basolateral membrane conductances of isolated hair cells. These studies have shown that hair cells possess a rich ensemble of ionic currents which determine their resting membrane potential and membrane properties. These include the inward calcium (I_{Ca}) (Eatock and Hutzler 1992; Fuchs et al. 1990; Hudspeth and Lewis 1988a; Lang and Correia 1989; Lewis and Hudspeth 1983; Ohmori 1984; Rennie and Ashmore 1991; Roberts et al. 1990) and anomalous rectifier (Ohmori 1984; Sugihara and Furukawa 1989; Fuchs and Evans 1990; Eatock and Hutzler 1992) currents and three outward potassium currents—the delayed rectifier (I_K) (Eatock and Hutzler 1992; Fuchs and Evans 1990; Housley et al. 1989; Kros and Crawford 1990; Lang and Correia 1989; Steinacker and Romero 1991, 1992), the transient rectifier (I_A) (Eatock and Hutzler 1992; Housley et al. 1989; Kros and Crawford 1990; Lang and Correia 1989; Murrow and Fuchs 1990; Rennie and Ashmore 1991; Steinacker and Romero 1992; Sugihara and Furukawa 1989), and the Ca^{2+}-activated rectifier ($I_{K(Ca)}$) (Eatock and Hutzler 1992; Fuchs and Evans 1990; Housley et al. 1989; Hudspeth and Lewis 1988a; Kros and Crawford 1990; Lang and Correia 1989; Lewis and Hudspeth 1983; Ohmori 1984; Rennie and Ashmore 1991; Roberts et al. 1990; Steinacker and Romero 1991, 1992; Sugihara and Furukawa 1989). There is also recent evidence that Type I vestibular hair cells possess a persistent outward current (Correia and Lang 1990; Eatock and Hutzler 1992; Rennie and Ashmore 1991) similar to the M-current previously described in bullfrog sympathetic neurons (Adams et al. 1982).

My results suggest that hair cell types in the bullfrog utriculus possess different complements of basolateral membrane conductances. Unfortunately, because of the large leakage conductance introduced by sharp microelectrodes during cell impalement, it is not possible to achieve more than a qualitative description of the basolateral membrane conductances of hair cells with conventional current-clamp recordings. In addition, these recordings cannot detect the contribution of small conductances nor distinguish the effects of slowly activating conductances from the rapid inactivation of more transient conductances. I can, however, infer the identify of many of these conductances from theoretical considerations and the steady-state and dynamic responses of hair cells to intracellular current.

On theoretical grounds I_{Ca} is found in all hair cells and is undoubtedly involved in Ca^{2+}-dependent transmitter release from hair cells to vestibular nerve afferents (Fuchs et al. 1990; Hudspeth and Lewis 1988a; Lang and Correia 1989; Lewis and Hudspeth 1983; Ohmori 1984; Roberts et

al. 1990). This inward current, however, would not be expected to be detected with conventional current-clamp recordings. One, it is only slightly activated near resting membrane potential. Two, it is small, representing only 10% of the total membrane current of semicircular canal hair cells (Housley et al. 1989; Lang and Correia 1989), and cannot usually be detected even in whole-cell recordings without pharmacologically blocking larger potassium currents. Calcium channels appear to have similar gating kinetics in all vestibular hair cells, displaying rapid (100–200 μs) activation and little or no inactivation to depolarizing voltages (Hudspeth and Lewis 1988a; Lang and Correia 1989; Lewis and Hudspeth 1983; Ohmori 1984; Roberts et al. 1990).

Utricular hair cells, like other hair cells, presumably possess a number of potassium currents. My results suggest that the identity of these currents is different in different hair cell types. Type B cells, in both the striolar and extrastriolar regions, have high R_N that dominate their voltage responses near resting membrane potential. The high R_N and passive responses of these cells to depolarizing and hyperpolarizing current also suggest that Type B cells have few, if any, membrane conductances activated near resting membrane potential. At larger depolarizing potentials, potentials at which outward potassium channels would presumably be strongly activated, these cells continued to exhibit slow responses with little outward rectification. This suggests that the steady-state *I-V* relations of these hair cells are dominated by I_K, the activation kinetics of which are considerably slower than other potassium currents (Fuchs and Evans 1990; Lang and Correia 1989; Steinacker and Romero 1991).

Type C cells have low R_N and near-linear *I-V* relations, suggesting that they possess a persistent potassium conductance. The only persistent potassium conductance previously reported in hair cells is that seen in Type I hair cells in the pigeon (Correia and Lang 1990), guinea pig (Rennie and Ashmore 1991), and rat (Eatock and Hutzler 1992). These hair cells, unlike Type II hair cells in the same preparations, display large, persistent outward currents near their resting membrane potentials with properties similar to those of the M-current described in bullfrog sympathetic neurons (Adams et al. 1982). In sympathetic neurons the time-dependent opening of M-channels introduces considerable outward rectification into the steady-state *I-V* relations of bullfrog sympathetic neurons (Adams et al. 1982). The M-current of hair cells, however, appears to activate and deactivate much more rapidly than that in sympathetic neurons (Correia and Lang 1990; Eatock and Hutzler 1992) and time-dependent relaxation of this current is not observed for voltage steps more positive than the potassium equilibrium potential (Correia and Lang 1990). This would tend to reduce outward rectification, resulting in a linear steady-state *I-V* relation. In response to hyperpolarizing current steps, the M-current would be expected to decrease, resulting in a sag in potential dependent on the proximity to the potassium equilibrium potential (Correia and Lang 1990; Eatock and Hutzler 1992; Rennie and Ashmore 1991).

Type C cells also display rapid responses to depolarizing currents, suggesting that they possess a potassium current with fast activation kinetics. The size of these responses did not decrease at large positive potentials, suggesting that $I_{K(Ca)}$ was not involved in their generation. They were diminished, however, when Type C cells were held at depolarized potentials with constant current injection. This current is therefore likely to be I_A, which in other preparations reaches a steady-state value within 5–10 ms during depolarizing voltage steps. Activation of this current, unlike other potassium currents, is facilitated when a large depolarizing step is applied from hyperpolarized potentials (Hudspeth and Lewis 1988a; Lewis and Hudspeth 1983). At depolarizing potentials, I_A is either largely (Lang and Correia 1989; Sugihara and Furukawa 1989) or completely (Hudspeth and Lewis 1988a; Lewis and Hudspeth 1983) inactivated.

Type F cells, like Type B cells, have high R_N, suggesting that they have few, if any, membrane conductances activated at or below resting membrane potential. For small depolarizing currents these cells displayed slow active responses, suggesting that they are dominated by I_K current. This is consistent with the nearly linear *I-V* relations of these cells for small depolarizing currents. At larger depolarizing potentials the peaks of Type F cells decreased in size for voltages more positive than −10 mv, suggesting that these cells may also possess $I_{K(Ca)}$. In cells dominated by this current, outward current grows with increasing depolarization until the increased driving force on potassium is offset by the decreased driving force on calcium entry. Thus there is a diminution of the outward current for potentials near the calcium equilibrium potential, resulting in an "N-shaped" *I-V* relation. Because the *I-V* relations of Type F cells merely saturated rather than exhibiting such pronounced N-shaped relations it is likely that this current, as in pigeon semicircular canal hair cells (Lang and Correia 1989), is small.

Type E hair cells, unlike other utricular hair cells, are electrically resonant. High-quality electrical resonance in auditory and vibratory hair cells has universally been correlated with the presence of $I_{K(Ca)}$ (Hudspeth and Lewis 1988a; Lewis and Hudspeth 1982; Steinacker and Romero 1992; Sugihara and Furukawa 1989). $I_{K(Ca)}$ is the largest ionic current in these cells, dominating their steady-state *I-V* relations positive to their resting membrane potential. Moreover, the activation kinetics of $I_{K(Ca)}$ in individual hair cells varies and is correlated with the resonant frequency of electrical oscillations. Thus hair cells with higher resonant frequencies have faster Ca^{2+}-activated potassium channels (Art and Fettiplace 1987; Fuchs and Evans 1990; Roberts et al. 1986). Unlike cells dominated by $I_{K(Ca)}$, resonant Type E cells have small and highly damped oscillations. They therefore presumably possess other, Ca^{2+}-independent, potassium currents (Steinacker and Romero 1992; Sugihara and Furukawa 1989). These currents would increase the membrane conductance of these cells, stabilizing their membrane potential and reducing the amplitude and quality of electrical oscillations. One of these currents may be I_K, which has been shown to be block the production of symmetrical electrical resonance in toadfish sacculus hair cells (Steinacker and Romero 1992). A small number of Type E cells had slow, spikelike responses. In these cells an increasing depolarization is observed during depolarizing current steps, indicative of I_A inactivation (Sugihara and

Furukawa 1989). This depolarization is not observed when these cells are held at depolarized potentials with constant current injection, lending further support to the notion that an A-type current is involved. These cells also exhibit very slow hyperpolarizations at the termination of current steps, suggesting that they also possess I_K, which, when activated by a maintained or low-frequency stimulus, is slow to inactivate (Fuchs and Evans 1990; Housley et al. 1989; Lang and Correia 1989; Steinacker and Romero 1991).

Type E cells also display a pronounced inward rectification at potentials more negative than −100 mV. One possible mechanism for this change in resistance is activation of an inward rectifier current. Similar inward rectifier currents have been observed in chick vestibular cells (Ohmori 1984) and electrically resonant hair cells in the goldfish sacculus (Sugihara and Furukawa 1989) and chick cochlea (Fuchs and Evans 1990). Hair cells exhibiting inward rectification had similar resting membrane potentials as those that did not, suggesting that this inward rectifier current is probably permeable to both sodium and potassium ions (Sugihara and Furukawa 1989).

Functional organization of the utricular macula

There is a regional organization of the utricular macula with afferents innervating the central, or striolar, zone of the endorgan having higher gains and more phasic response dynamics than those supplying the peripheral, or extrastriolar, zone (Baird and Lewis 1986; Goldberg et al. 1985, 1990). Morphological studies also indicate that the innervations of these macular zones are relatively independent (Baird and Schuff 1994). It is therefore of interest to ask whether hair cells in these regions differ in their physiological response properties. My results reveal that the responses of striolar hair cells to intracellular current differ in several respects from those of hair cells in extrastriolar regions (see below). Morphological studies in both the bullfrog (Baird and Schuff 1994) and the chinchilla (Fernandez et al. 1990) further demonstrate that afferent innervation patterns in a juxtastriolar zone, located immediately adjacent to the medial striola, differ from those in more peripheral extrastriolar regions, suggesting that hair cells in the extrastriolar regions may also differ in their physiological response properties. My results show little support for this suggestion. The number of Type B cells recorded in this study was, however, small and these cells were all from the striolar and juxtastriolar zones.

Type B cells in the striolar and extrastriolar regions have similar response properties. These cells have high R_N that make them highly sensitive to small receptor potentials but limit their bandwidths to natural stimulation around their resting membrane potentials. The responses of these cells appear to be dominated by I_K. This current is slow to turn on and is not likely to be activated during rapid or high-frequency stimulation. When activated by a maintained or low-frequency stimulus it is also slow to inactivate. Functionally, this implies that these cells are slow to repolarize and slow to return to prestimulus conditions. They are, however, well suited to encode static gravity and tonic head and body movements.

Hair cells restricted to the striolar region differ in several respects from those of Type B cells. Type C cells, for example, have low R_N, greatly increasing their slope conductance to potentials around their resting membrane potential. This would make these cells less sensitive to small receptor potentials. At the same time, it would extend their dynamic range, enabling them to encode a wider range of stimulus amplitudes. These cells also possess faster outward currents than Type B cells, enabling them to better respond to higher frequency stimulation. Thus they are well suited for encoding phasic head and body movements over a wide range of amplitudes and frequencies.

Type E cells have high R_N that increase their sensitivity to small receptor potentials but limit their bandwidths to natural stimulation. They also, however, display strong outward rectification, markedly increasing their slope conductances with increasing depolarization. This rectification increases the corner frequencies of these cells for larger stimuli, allowing hair cells to modulate transmitter release at frequencies higher than their membrane time constant. Type E cells, unlike other utricular hair cells, are also electrically resonant. Hair cells in the bullfrog can therefore be classified, as in other auditory and vestibular endorgans (Correia et al. 1989; Fuchs and Evans 1990; Fuchs et al. 1988; Steinacker and Romero 1991, 1992; Sugihara and Furukawa 1989), into resonant and nonresonant classes. This resonance presumably allows these cells, as in auditory and vibratory endorgans, to encode stimulus frequency (Ashmore 1983; Crawford and Fettiplace 1981; Fuchs et al. 1988; Hudspeth and Lewis 1988a; Lewis and Hudspeth 1983; Pitchford and Ashmore 1987).

Type E cells are selectively innervated by one class of utricular afferents (Baird and Schuff 1994), suggesting that at least some utricular afferents primarily convey frequency information to the CNS. The damped resonance of Type E cells may also allow these cells to encode temporal aspects of the stimulus signal. In auditory and vibratory endorgans, resonance in individual hair cells is restricted to a narrow range of frequencies and there is a tonotopic mapping of frequency across the endorgan. Afferents innervating these cells have very restricted innervation patterns, strongly phase-locking their discharge to the oscillations of hair cells and allowing them to transmit precise information about stimulus frequency to the CNS. Vestibular organs, by reducing the quality of electrical resonance, may allow hair cells to respond to a greater range of frequencies. Afferents innervating these cells can then achieve phase-locking over a wider frequency range. Resonating hair cells in gravisensitive endorgans may also encode both the transient and envelope of a stimulus signal (Steinacker and Romero 1991).

The functional role of Type F cells is less clear. Unlike Type E cells, they are not selectively innervated by utricular afferents and make up only a small percentage of the total innervation of striolar afferents (Baird and Schuff 1994). These cells resemble Type B cells in having high R_N and slow voltage responses. They would thus seem well suited for encoding tonic head and body movements. Like Type E cells, however, the slope conductance of these cells decreases markedly with increasing depolarization, increasing their corner frequencies for larger stimulation. They might therefore complement the responses of Type B cells, encoding small head and body movements over a somewhat higher range of frequencies.

In conclusion, the bullfrog utriculus is highly organized to extract static and dynamic information about head and

body movement. Type B cells in the striolar and extrastriolar regions of this endorgan are well suited for encoding static gravity and low-frequency linear accelerations. Hair cells restricted to the striolar region, on the other hand, are specialized to encode higher frequency information. These hair cells possess faster ionic currents and, in the case of Type E cells, are electrically tuned to further enhance their high-frequency sensitivities. As we shall see in the companion paper (Baird 1994), hair cells in the striolar and extrastriolar regions also differ in their responses to mechanical stimulation. These differences, unlike the differences discussed here, appear to be shaped by the morphological properties of the hair bundle and the adaptation kinetics of the transduction channel.

The bullfrog, unlike the mammal, possesses only Type II hair cells (Lindeman, 1969; Wersall and Bagger-Sjoback 1974), which differ markedly in kinociliary and stereociliary morphology (Lewis and Li 1975). These differences are correlated with the physiological responses of these hair cells to intracellular current. A similar association may also be applicable to higher vertebrates. Recent studies have shown that the longest stereocilia of Type I and Type II hair cells in mammals display regional variations in morphology (Lapeyre et al. 1992). It is not known whether these regional variations are associated with differences in hair bundle physiology. It is, however, possible that such variations, more subtle than those involved in the separation of hair cells into Type I and Type II varieties, may be correlated with differences in hair cell physiology in mammalian preparations.

I am grateful to N. R. Schuff for figure preparation and assistance during electrophysiological experiments and to B. Smith for manuscript preparation.

Funding for this work was provided by National Institute of Deafness and Communicative Disorders Grants DC-00355 and DC02040, by National Aeronautics and Space Administration Grant NCC 2-651, and by grants from the Oregon Lions Sight and Hearing Foundation.

Address for reprint requests: R. A. Baird, R. S. Dow Neurological Sciences Institute, Good Samaritan Hospital and Medical Center, 1120 NW 20th Avenue, Portland, OR 97209.

Received 24 February 1993; accepted in final form 14 October 1993.

REFERENCES

ADAMS, P. R., BROWN, D. A., AND CONSTANTI, A. M-currents and other potassium currents in bullfrog sympathetic neurons. *J. Physiol. Lond.* 330: 537–572, 1982.

ART, J. J., CRAWFORD, A. C., AND FETTIPLACE, R. Electrical resonance and membrane currents in turtle cochlear hair cells. *Hear. Res.* 22: 31–36, 1986.

ART, J. J. AND FETTIPLACE, R. Variation of membrane properties in hair cells isolated from the turtle cochlea. *J. Physiol. Lond.* 385: 207–242, 1987.

ASHMORE, J. F. Frequency tuning in a frog vestibular organ. *Nature Lond.* 304: 536–538, 1983.

BAIRD, R. A. Morphological and electrophysiological properties of hair cells in the bullfrog utriculus. *Ann. NY Acad. Sci.* 656: 12–26, 1992.

BAIRD, R. A. Comparative transduction and tuning mechanisms of hair cells in the bullfrog utriculus. II. Sensitivity and response dynamics to mechanical displacement. *J. Neurophysiol.* 71: 685–705, 1994.

BAIRD, R. A., DESMADRYL, G. FERNANDEZ, C., AND GOLDBERG, J. M. The vestibular nerve of the chinchilla. II. Relation between afferent response properties and peripheral innervation patterns in the semicircular canals. *J. Neurophysiol.* 60: 182–203, 1988.

BAIRD, R. A. AND LEWIS, E. R. Correspondences between afferent innervation patterns and response dynamics in the bullfrog utricle and lagena. *Brain Res.* 369: 48–64, 1986.

BAIRD, R. A. AND SCHUFF, N. R. Comparative transduction mechanisms of hair cells in the bullfrog utricle. *Soc. Neurosci. Abstr.* 16: 733, 1990.

BAIRD, R. A. AND SCHUFF, N. R. Transduction mechanisms of hair cells in the bullfrog utricle. *Assoc. Res. Otolaryngol. Abstr.* 14: 38, 1991.

BAIRD, R. A. AND SCHUFF, N. R. Peripheral innervation patterns of vestibular nerve afferents in the bullfrog utriculus. *J. Comp. Neurol.* In press.

BAIRD, R. A., TORRES, M. A., AND SCHUFF, N. R. Hair cell regeneration in the bullfrog vestibular otolith organs following aminoglycoside ototoxicity. *Hear. Res.* 65: 164–174, 1993.

BOYLE, R., CAREY, J. P., AND HIGHSTEIN, S. M. Morphological correlates of response dynamics and efferent stimulation in horizontal semicircular canal afferents of the toadfish, *Opsanus tau*. *J. Neurophysiol.* 66: 1504–1521, 1991.

BROWNELL, W. E., BADER, C. R., BERTRAND, D., AND DE RIBAUPIERRE, Y. Evoked mechanical responses in isolated cochlear outer hair cells. *Science Wash. DC* 227: 194–196, 1985.

COREY, D. P. AND HUDSPETH, A. J. Ionic basis of the receptor potential in vertebrate hair cell. *Nature Lond.* 281: 657–677, 1979.

COREY, D. P. AND HUDSPETH, A. J. Kinetics of the receptor current in bullfrog saccular hair cells. *J. Neurosci.* 3: 962–976, 1983.

CORREIA, M. J., CHRISTENSEN, B. N., MOORE, L. E. AND LANG, D. G. Studies of solitary semicircular canal hair cells in the adult pigeon. I. Frequency- and time-domain analysis of active and passive membrane properties. *J. Neurophysiol.* 62: 924–934, 1989.

CORREIA, M. J. AND LANG, D. G. An electrophysiological comparison of solitary type I and type II vestibular hair cells. *Neurosci. Lett.* 116: 106–111, 1990.

CRAWFORD, A. C. AND FETTIPLACE, R. An electrical tuning mechanism in turtle cochlear hair cells. *J. Physiol. Lond.* 312: 377–412, 1981.

DALLOS, P. Neurobiology of cochlear inner and outer hair cells: intracellular recordings. *Hear. Res.* 22: 185–198, 1986.

EATOCK, R. A., COREY, D. P., AND HUDSPETH, A. J. Adaptation of mechanoelectric transduction in hair cells of the bullfrog's sacculus. *J. Neurosci.* 7: 2821–2836, 1987.

EATOCK, R. A. AND HUTZLER, M. J. Ionic currents of mammalian vestibular hair cells. *Ann. NY Acad. Sci.* 656: 58–74, 1992.

FERNANDEZ, C., GOLDBERG, J. M., AND BAIRD, R. A. The vestibular nerve of the chainhcilola. III. Peripheral innervation patterns of the utricular macula. *J. Neurophysiol.* 63: 767–804, 1990.

FUCHS, P. A. AND EVANS, M. G. Potassium currents in hair cells isolated from the cochlea of the chick. *J. Physiol. Lond.* 429: 529–551, 1990.

FUCHS, P. A., EVANS, M. G., AND MURROW, B. W. Calcium currents in hair cells isolated from the cochlea of the chick. *J. Physiol. Lond.* 429: 553–568, 1990.

FUCHS, P. A., NAGAI, T., AND EVANS, M. G. Electrical tuning in hair cells isolated from chick cochlea. *J. Neurosci.* 8: 2460–2467, 1988.

GOLDBERG, J. M., BAIRD, R. A., AND FERNANDEZ, C. Morphophysiological studies of the mammalian vestibular labyrinth. In: *Progress in Clinical and Biological Research. Contemporary Sensory Neurobiology*, edited by M. J. Correia and A. A. Perachio. New York: Liss, 1985, vol. 176, p. 231–245.

GOLDBERG, J. M., DESMADRYL, G., BAIRD, R. A., AND FERNANDEZ, C. The vestibular nerve in the chinchilla. V. Relation between afferent response properties and peripheral innervation patterns in the utricular macula. *J. Neurophysiol.* 63: 781–790, 1990.

GOLDBERG, J. M., SMITH, C. E., AND FERNANDEZ, C. The relation between discharge regularity and responses to externally applied galvanic currents in vestibular-nerve afferents of the squirrel monkey. *J. Neurophysiol.* 51: 1236–1256, 1984.

HAMILL, O. P., MARTY, A., NEHER, E., SAKMANN, B., AND SIGWORTH, F. J. Improved patch-clamp techniques for high resolution current recording from cells and cell-free membrane patches. *Pfluegers Arch.* 393: 254–261, 1981.

HILLMAN, D. E. AND MCLAREN, J. W. Displacement configuration of semicircular canal cupulae. *Neuroscience* 4: 1989–2000, 1979.

HOLTON, T. AND HUDSPETH, A. J. The transduction channel of hair cells from the bullfrog characterized by noise analysis. *J. Physiol. Lond.* 375: 195–227, 1986.

HILLMAN, D. E. AND MCLAREN, J. W. Displacement configuration of semicircular canal cupulae. *Neuroscience* 4: 1989–2000, 1979.

HOLTON, T. AND HUDSPETH, A. J. The transduction channel of hair cells from the bullfrog characterized by noise analysis. *J. Physiol. Lond.* 375: 195–227, 1986.

HONRUBIA, V., HOFFMAN, L. F., SITKO, S. T., AND SCHWARTZ, I. R. Ana-

tomic and physiological correlates in bullfrog vestibular nerve. *J. Neurophysiol.* 61: 688–701, 1989.

HONRUBIA, V., SITKO, S. T., KIMM, J., BETTS, W., AND SCHWARTZ, I. R. Physiological and anatomical characteristics of primary vestibular afferent neurons in the bullfrog. *Int. J. Neurosci.* 15: 197–206, 1981.

HORIKAWA, K. AND ARMSTRONG, W. E. A versatile means of intracellular labeling: injection of biocytin and its detection with avidin conjugates. *J. Neurosci. Methods* 25: 1–11, 1988.

HOUSLEY, G. D., NORRIS, C. H., AND GUTH, P. S. Electrophysiological properties and morphology of hair cells isolated from the semicircular canal of the frog. *Hear. Res.* 38: 259–276, 1989.

HOWARD, J., ROBERTS, W. M., AND HUDSPETH, A. J. Mechanoelectrical transduction by hair cells. *Annu. Rev. Biophys. Chem.* 17: 99–124, 1988.

HUDSPETH, A. J. The cellular basis of hearing: the biophysics of hair cells. *Science Wash. DC* 230: 745–752, 1986.

HUDSPETH, A. J. AND COREY, D. P. Sensitivity, polarity and conductance change in the response of vertebrate hair cells to controlled mechanical stimuli. *Proc. Natl. Acad. Sci. USA* 74: 2407–2411, 1977.

HUDSPETH, A. J. AND LEWIS, R. S. Kinetic analysis of voltage- and ion-dependent conductances in saccular hair cells of the bullfrog, *Rana catesbeiana*. *J. Physiol. Lond.* 400: 237–274, 1988a.

HUDSPETH, A. J. AND LEWIS, R. S. A model for electrical resonance and frequency tuning in saccular hair cells of the bullfrog, *Rana catesbeiana*. *J. Physiol. Lond.* 400: 275–297, 1988b.

KOYAMA, H., LEWIS, E. R., LEVERENZ, E. L., AND BAIRD, R. A. Acute seismic sensitivity in the bullfrog ear. *Brain Res.* 250: 168–172, 1982.

KROS, C. J. AND CRAWFORD, A. C. Potassium currents in inner hair cells isolated from the guinea-pig cochlea. *J. Physiol. Lond.* 421: 263–291, 1990.

LANG, D. G. AND CORREIA, M. J. Studies of solitary semicircular canal hair cells in the adult pigeon. II. Voltage-dependent ionic conductances. *J. Neurophysiol.* 62: 935–945, 1989.

LAPEYRE, P., GUILHAUME, A., AND CAZALS, Y. Differences in hair bundles associated with Type I and Type II vestibular hair cells of the guinea pig saccule. *Acta Otolaryngol. Stockh.* 112: 635–642, 1992.

LEWIS, E. R., BAIRD, R. A., LEVERENZ, E. L., AND KOYAMA, H. Inner ear: dye injection reveals peripheral origins of specific sensitivities. *Science Wash. DC* 215: 1641–1643, 1982.

LEWIS, E. R. AND LI, C. W. Hair cell types and distributions in the otolithic and auditory organs of the bullfrog. *Brain Res.* 83: 35–50, 1975.

LEWIS, R. S. AND HUDSPETH, A. J. Voltage and ion-dependent conductances in solitary vertebrate hair cells. *Nature Lond.* 304: 538–541, 1983.

LIM, D. J. Morphological and physiological correlates in cochlear and vestibular sensory epithelia. In: *Scanning Electron Microscopy*, edited by O. Johari and R. P. Becker. Chicago: IIT Research Institute, 1976, vol. 5, p. 269–276.

LINDEMAN, H. H. Studies on the morphology of the sensory regions of the vestibular apparatus. *Ergeb. Anat. Entwicklungsgesch.* 42: 1–113, 1969.

MARTY, A. AND NEHER, E. Tight-seal whole-cell recording. In: *Single Channel Recording*, edited by B. Sakmann and E. Neher. New York: Plenum, 1983, p. 107–122.

MCLAREN, J. W. AND HILLMAN, D. E. Displacement of the semicircular canal cupula during sinusoidal rotation. *Neuroscience* 4: 2001–2008, 1979.

MILLER, R. G., JR. Developments in multiple comparisons, 1966–1977. *J. Am. Statist. Assoc.* 72: 779–788, 1977.

MURROW, B. W. AND FUCHS, P. A. Preferential expression of transient potassium current (I_A) by "short" hair cells of the chick's cochlea. *Proc. R. Soc. Lond. B Biol. Sci.* 242: 189–195, 1990.

NUTALL, A. L. Influence of direct current on DC receptor potentials from cochlear inner hair cells in the guinea pig. *J. Acoust. Soc. Am.* 77: 165–175, 1985.

OHMORI, H. Studies of ionic currents in the isolated vestibular hair cells of the chick. *J. Physiol. Lond.* 350: 561–581, 1984.

PITCHFORD, S. AND ASHMORE, J. F. An electrical resonance in hair cells of the amphibian papilla of the frog *Rana temporaria*. *Hear. Res.* 27: 75–84, 1987.

RENNIE, K. J. AND ASHMORE, J. F. Ionic currents in isolated vestibular hair cells from the guinea-pig crista ampullaris. *Hear. Res.* 51: 279–291, 1991.

ROBERTS, W. M., HOWARD, J., AND HUDSPETH, A. J. Hair cells: transduction, tuning, and transmission in the inner ear. *Annu. Rev. Cell Biol.* 4: 63–92, 1988.

ROBERTS, W. M., JACOBS, R. A., AND HUDSPETH, A. J. Colocalization of ion channels involved in frequency selectivity and synaptic transmission at presynaptic active zones of hair cells. *J. Neurosci.* 10: 3664–3684, 1990.

ROBERTS, W. M., ROBLES, L., AND HUDSPETH, A. J. Correlation between the kinetic properties of ionic channels and the frequency of membrane-potential resonance in hair cells of the bullfrog. In: *Auditory Frequency Selectivity*, edited by B. C. J. Moore and R. D. Patterson. New York: Plenum, 1986, p. 89–95.

RUSSELL, I. J., CODY, A. R., AND RICHARDSON, G. P. The responses of inner and outer hair cells in the basal turn of the guinea-pig cochlea and in the mouse cochlea grown in vitro. *Hear. Res.* 22: 199–216, 1986.

STEINAKER, T. AND ROMERO, A. Characterization of voltage-gated and calcium-activated potassium currents in toadfish saccular hair cells. *Brain Res.* 556: 22–32, 1991.

STEINAKER, T. AND ROMERO, A. Voltage-gated potassium current and resonance in the toadfish saccular hair cell. *Brain Res.* 574: 229–236, 1992.

STEWART, W. W. Functional connections between cells as revealed by dye-coupling with a highly fluorescent naphthalimide tracer. *Cell* 14: 741–759, 1978.

SUGIHARA, I. AND FURUKAWA, T. Morphological and functional aspects of two different types of hair cells in the goldfish sacculus. *J. Neurophysiol.* 62: 1330–1342, 1989.

TURNER, R. G., MURASKI, A. A., AND NIELSEN, D. W. Cilium length: influence on neural tonotopic organization. *Science Wash. DC* 213: 1519–1521, 1981.

WERSALL, J. AND BAGGER-SJOBACK, D. Morphology of the vestibular sense organs. In: *Handbook of Sensory Physiology, Vestibular System: Basic Mechanisms*, edited by H. H. Kornhuber. New York: Springer-Verlag, 1974, pt. 1, vol. 6, p. 123–170.